Distinct hypothalamic control of same- and opposite-sex mounting behaviour in mice

https://doi.org/10.1038/s41586-020-2995-0

Received: 17 December 2019

Accepted: 22 September 2020

Published online: 2 December 2020

Check for updates

Tomomi Karigo[1], Ann Kennedy[1,4], Bin Yang[1], Mengyu Liu[1], Derek Tai[1,5], Iman A. Wahle[2] & David J. Anderson[1,3] ✉

Animal behaviours that are superficially similar can express different intents in different contexts, but how this flexibility is achieved at the level of neural circuits is not understood. For example, males of many species can exhibit mounting behaviour towards same- or opposite-sex conspecifics[1], but it is unclear whether the intent and neural encoding of these behaviours are similar or different. Here we show that female- and male-directed mounting in male laboratory mice are distinguishable by the presence or absence of ultrasonic vocalizations (USVs)[2–4], respectively. These and additional behavioural data suggest that most male-directed mounting is aggressive, although in rare cases it can be sexual. We investigated whether USV^+ and USV^- mounting use the same or distinct hypothalamic neural substrates. Micro-endoscopic imaging of neurons positive for oestrogen receptor 1 (ESR1) in either the medial preoptic area (MPOA) or the ventromedial hypothalamus, ventrolateral subdivision (VMHvl) revealed distinct patterns of neuronal activity during USV^+ and USV^- mounting, and the type of mounting could be decoded from population activity in either region. Intersectional optogenetic stimulation of MPOA neurons that express ESR1 and vesicular GABA transporter (VGAT) ($MPOA^{ESR1\cap VGAT}$ neurons) robustly promoted USV^+ mounting, and converted male-directed attack to mounting with USVs. By contrast, stimulation of VMHvl neurons that express ESR1 ($VMHvl^{ESR1}$ neurons) promoted USV^- mounting, and inhibited the USVs evoked by female urine. Terminal stimulation experiments suggest that these complementary inhibitory effects are mediated by reciprocal projections between the MPOA and VMHvl. Together, these data identify a hypothalamic subpopulation that is genetically enriched for neurons that causally induce a male reproductive behavioural state, and indicate that reproductive and aggressive states are represented by distinct population codes distributed between $MPOA^{ESR1}$ and $VMHvl^{ESR1}$ neurons, respectively. Thus, similar behaviours that express different internal states are encoded by distinct hypothalamic neuronal populations.

To investigate whether female- and male-directed mounting in mice could be behaviourally discriminated, we first attempted to train a machine-learning-based classifier[5] to distinguish mounting in these two contexts (Fig. 1a, Methods). The performance of classifiers trained using pose features from mounting bouts alone was only slightly better than chance (63%) (Fig. 1b, c, Extended Data Fig. 1a, b). However, when trained using features extracted between −3 s and 1 s relative to mount initiation (at $t = 0$), classifier performance was improved to 78% (Extended Data Fig. 1e–g). This suggested that features from associated actions—more than from mounting itself—distinguish same-sex- and opposite-sex-directed mounting.

We therefore investigated which associated behaviours best discriminate the mounting of female versus male mice by male mice. Audio recordings revealed that female-directed mounts were invariably accompanied by USVs[2–4] (Fig. 1e, f, h, k, Supplementary Video 1), whereas most male-directed mounts were not (Fig. 1e–g, k, Supplementary Video 2; the rare exceptions are discussed below). In addition, female-directed mounts were followed usually by pelvic thrusting and intromission (Fig. 1h, l), whereas male-directed mounting was followed typically by attack (Fig. 1g, m). Finally, male-directed USV^- mounting was more frequent during initial social encounters when mice were socially inexperienced (day 1 in Fig. 1g, i, j, Extended Data Fig. 1h–j), and diminished as mice gained aggressive experience[6,7] (days 2 and 3 in Fig. 1n, o). These data suggest that most cases of naturally occurring female- and male-directed mounting in this mouse strain reflect underlying sexual and aggressive motivational states, respectively.

[1]Division of Biology and Biological Engineering, TianQiao and Chrissy Chen Institute for Neuroscience, California Institute of Technology, Pasadena, CA, USA. [2]Department of Computing and Mathematical Sciences, California Institute of Technology, Pasadena, CA, USA. [3]Howard Hughes Medical Institute, California Institute of Technology, Pasadena, CA, USA. [4]Present address: Department of Physiology, Feinberg School of Medicine Northwestern University, Chicago, IL, USA. [5]Present address: Touro University Nevada College of Osteopathic Medicine, Henderson, NV, USA. ✉e-mail: wuwei@caltech.edu

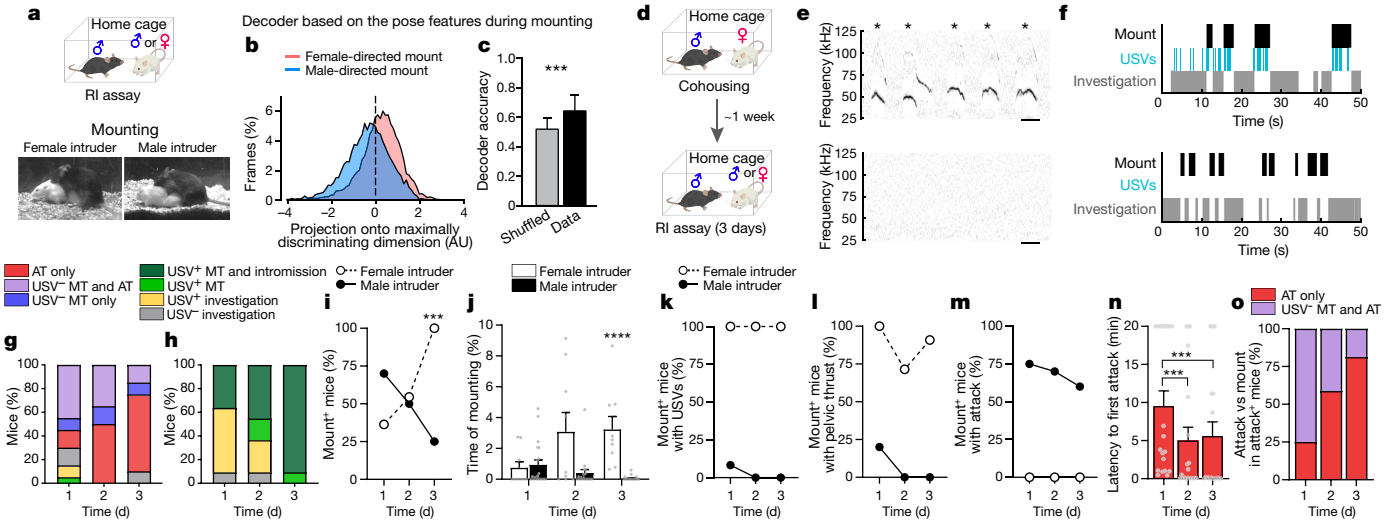

Fig. 1 | Female- and male-directed mounting are distinct male social behaviours. a, Experimental design (top) and representative video stills for female- and male-directed mounting (bottom). RI, resident–intruder. **b**, **c**, Decoding the sex of the intruder from female- versus male-directed mounting. AU, arbitrary units. **b**, Projection of mouse pose features from mounting bouts onto the maximally discriminating dimension of the decoder. **c**, Decoder accuracy compared with shuffled data. Fifty-four behaviour sessions, Mann–Whitney *U* test, $***P = 0.0004$. **d**, Schematic illustrating resident–intruder assay. Male intruder tests, $n = 20$; female intruder tests, $n = 11$. **e**, Representative spectrograms during female-directed (top) and male-directed (bottom) mounting. Scale, 100 ms. Asterisks indicate USV syllables. **f**, Representative raster plots indicating mount, USV and investigation episodes during interaction with female (top) or male (bottom) intruder. **g**, **h**, Distribution of social behaviours by a male mouse that was initially naive to male, across three consecutive days with a male (**g**) or female (**h**) intruder. See Extended Data Fig. 1h–j for details. AT, attack; MT, mount. **i**, **j**, Fraction of mice exhibiting mounting (**i**) and time spent mounting (**j**) on each test day. **i**, Fisher's test, $***P = 0.0002$; **j**, Kruskal–Wallis test, $****P < 0.0001$. **k**–**m**, Fraction of mice exhibiting mounting with USVs (**k**), pelvic thrust (**l**) or attack (**m**) on each test day. **n**, **o**, Quantification of behaviours towards male intruders on each test day. **n**, Latency to first attack (Methods). $n = 20$, Friedman test, $***P = 0.0003$, 0.0002. **o**, Fraction of mice exhibiting USV⁻ mount plus attack versus attack only. Data are mean ± s.e.m. All statistical tests are two-sided and corrected for multiple comparisons when necessary (Supplementary Table 2).

We investigated next how the hypothalamus encodes these two forms of mounting. In principle, female- and male-directed mounting could reflect the presence of behaviour-specific neurons that are either common or distinct (Extended Data Fig. 1k); alternatively, the two forms of mounting could reflect a more general encoding of aggressive and sexual internal states. ESR1⁺ neurons in both the MPOA and VMHvl have previously been implicated in male mounting[8–12]. To directly compare activity in these two populations during female- and male-directed mounting in the same mice, we performed simultaneous bulk calcium measurements in MPOA^{ESR1} and VMHvl^{ESR1} neurons using fibre photometry[13] (Fig. 2a, b, Extended Data Fig. 2, Methods). The activity in the former area was relatively higher during USV⁺ mounting, whereas activity in the latter area trended higher during USV⁻ mounting (Fig. 2c, d). We observed a similar relationship during other phases of female- versus male-directed social behaviour (Extended Data Fig. 3).

Notably, in two out of ten individual male mice (no. 629 and no. 634), activity during male-directed mounting resembled that typically observed during female-directed mounting—that is, activity was relatively higher in MPOA^{ESR1} than in VMHvl^{ESR1} neurons (Extended Data Fig. 4b, c, g, h). Furthermore, in both cases male-directed mounting was accompanied by USVs (Extended Data Fig. 4d, e). These rare examples may reflect mistaken sex identification[14] and/or male-directed affiliative (that is, bisexual) behaviour (Supplementary Note 2), and indicate that neural responses in these nuclei are not simply sensory representations of intruder sex.

The quantitative differences in bulk ESR1⁺ neuronal activity in each nucleus during sexual (USV⁺) versus aggressive (USV⁻) mounting (Fig. 2d) could reflect differences in the activity of the same neurons or the activation of different subsets of ESR1⁺ neurons[6,15,16]. To distinguish these alternatives, we performed single-cell-resolution calcium imaging of ESR1⁺ neurons using head-mounted micro-endoscopes[17], in either the MPOA or VMHvl[6], in freely behaving mice (Fig. 2e, Methods). To our knowledge, the single-cell-resolution imaging of MPOA activity during social behaviours has not previously been reported.

In the MPOA (as in the VMHvl[6]), we observed that distinct populations of ESR1⁺ neurons responded during female- and male-directed social interactions (Fig. 2f, Extended Data Fig. 5a–h). However female-preferring neurons outnumbered male-preferring neurons by twofold in the MPOA (18% versus 9%) (Fig. 2g left)—the reverse of the ratio in the VMHvl (12% versus 29%) (Fig. 2g right). In both structures, much of the variance in population activity was explained by intruder sex (30–52%) (grey bars in Fig. 2h), although in the MPOA a higher fraction of the variance was explained by behaviour (57%,) (pink and blue bars in Fig. 2h) than was the case in the VMHvl (about 37%) (Methods).

To further investigate the relationship between neural activity and behaviour, we performed a frame-by-frame annotation of behaviour in synchronously acquired video recordings[5] (Extended Data Fig. 6a, b). Both the MPOA and VMHvl contained distinct populations of neurons that were activated at the onset of USV⁺ and USV⁻ mounting, respectively (Fig. 2i, j). However, overall the relative activity of each cell during mounting and investigation was highly correlated—for intruders of a given sex—in both the MPOA ($R^2 = 0.61$–0.71) (Extended Data Fig. 5i, j) and VMHvl ($R^2 = 0.77$–0.88) (Extended Data Fig. 5k, l), and was poorly correlated across different sexes (Extended Data Fig. 5a–h). A small proportion of neurons was preferentially activated (more than 2σ) during mounting but not sniffing (green or blue points and sectors in Extended Data Fig. 5i–l and 5m–p, respectively). This suggests that the activity observed during USV⁺ or USV⁻ mounting is not simply a reflection of the sex of the intruder (which would also contribute to neuronal activation during sniffing), but that at least some neurons are selectively activated during USV⁺ or USV⁻ mounting behaviour. However, cells that responded during both behaviours were more numerous and more strongly activated than those that responding during one behaviour only (grey points in Extended Data Fig. 5i–l, grey sectors in Extended Data Fig. 5m–p).

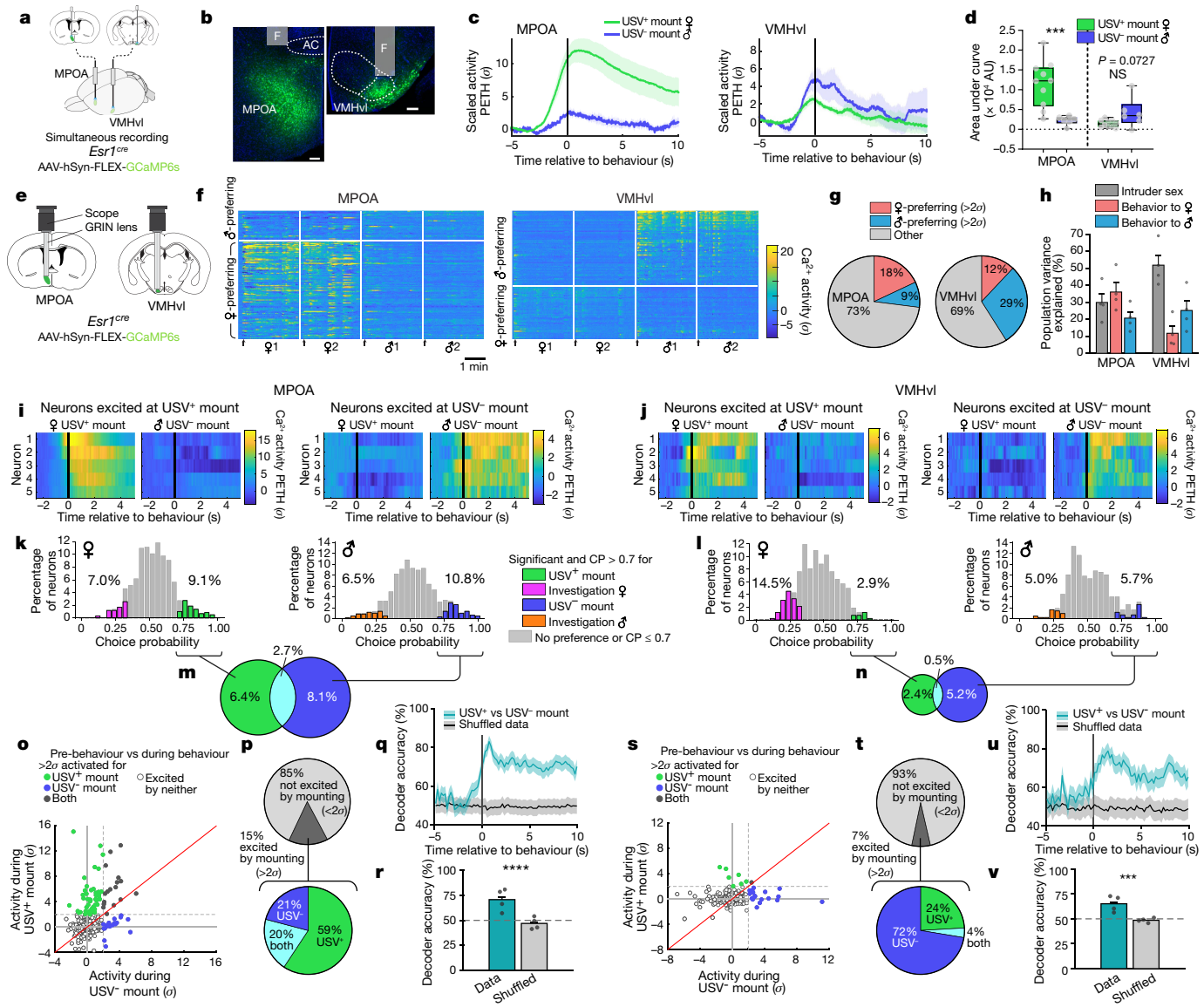

Fig. 2 | Distinct neural representations of USV⁺ and USV⁻ mounting in MPOA^{ESR1} and VMHvl^{ESR1} neurons. a, Schematic illustrating dual-site fibre photometry. **b**, Representative GCaMP6s expression and optic fibre tract. Scale bars, 100 µm. $n = 10$. AC, anterior commissure; F, optic fibre tract. See Extended Data Fig. 2c, e for examples from control experiments. **c**, **d**, Averaged calcium signals in MPOA^{ESR1} and in VMHvl^{ESR1} aligned to mount onset (Methods). PETH, peri-event time histograms. **d**, Integrated activity during mounting. ***$P = 0.001$. USV⁺ mount, $n = 10$; USV⁻ mount, $n = 6$. **e**, Schematic of micro-endoscopic calcium imaging. GRIN, gradient index. **f**, Representative calcium activity raster during social encounters, sorted by intruder sex preference and response magnitude. Arrows, intruder introduction. **g**, Fraction of female- and male-preferring MPOA^{ESR1} and VMHvl^{ESR1} neurons. **h**, Main sources of variance in population activity (Methods). $n = 4$ for each region. **i**, **j**, Neural activity of example mount-activated neurons, shown as PETHs (normalized to 2.5 to 1.5 s before mount onset). Each pair of rasters is from the same neuron. **k**, **l**, Choice probabilities (CP) for female- or male-directed investigation versus USV⁺ or USV⁻ mounting (coloured bars indicate significance, Methods). **m**, **n**, Proportion of cells showing significance (Methods) and choice probability >0.7 for USV⁺ mounting, USV⁻ mounting or both. **o**, **p**, **s**, **t**, Average activity per neuron (σ, relative to pre-mount activity) during USV⁺ versus USV⁻ mounting. **o**, **s**, Scatter plots. **p**, **t**, Proportion of cells excited (>2σ) during mounting. **q**, **r**, **u**, **v**, Accuracy of time-evolving (**q**, **u**) or frame-wise (**r**, **v**) decoders predicting USV⁺ from USV⁻ mounting, trained on neural activity. $n = 4$, ****$P < 0.0001$. **d**, **r**, **v**, Mann–Whitney U test. Data are mean ± s.e.m., except in box plots (**d**), in which centre lines indicate medians, box edges represent the interquartile range and whiskers denote minimal and maximal values. All statistical tests are two-sided and corrected for multiple comparisons when necessary (Supplementary Table 2).

To further investigate the specificity of the behavioural responses, we computed the choice probability of each neuron for mounting (USV⁺ or USV⁻) versus investigation (sniffing)[6]. The choice probability of a neuron indicates how accurately the activity of the neuron can predict whether mounting or investigation is occurring, during each annotated frame in which the neuron is active[18]. In both the VMHvl and MPOA, 3–11% of ESR1⁺ neurons exhibited a choice probability of more than 0.7 for sexual (USV⁺) or aggressive (USV⁻) mounting, respectively (relative to investigation), that was substantially higher (over 2σ) compared to shuffled behavioural annotations (Fig. 2k, l, Methods). This confirms that both nuclei contain some cells that are tuned for mounting, independently of the sex of the intruder. However, these cells appeared to lie at the extremes of a continuum of relative 'tuning' for mounting versus investigation. Nevertheless, in both the MPOA and VMHvl, there was minimal overlap between USV⁺-mount-tuned and USV⁻-mount-tuned cells identified by choice probability analysis (Fig. 2m, n). Similarly, in both nuclei the ESR1⁺ subpopulations that were preferentially activated (more than 2σ) during the two types of mounting were largely distinct

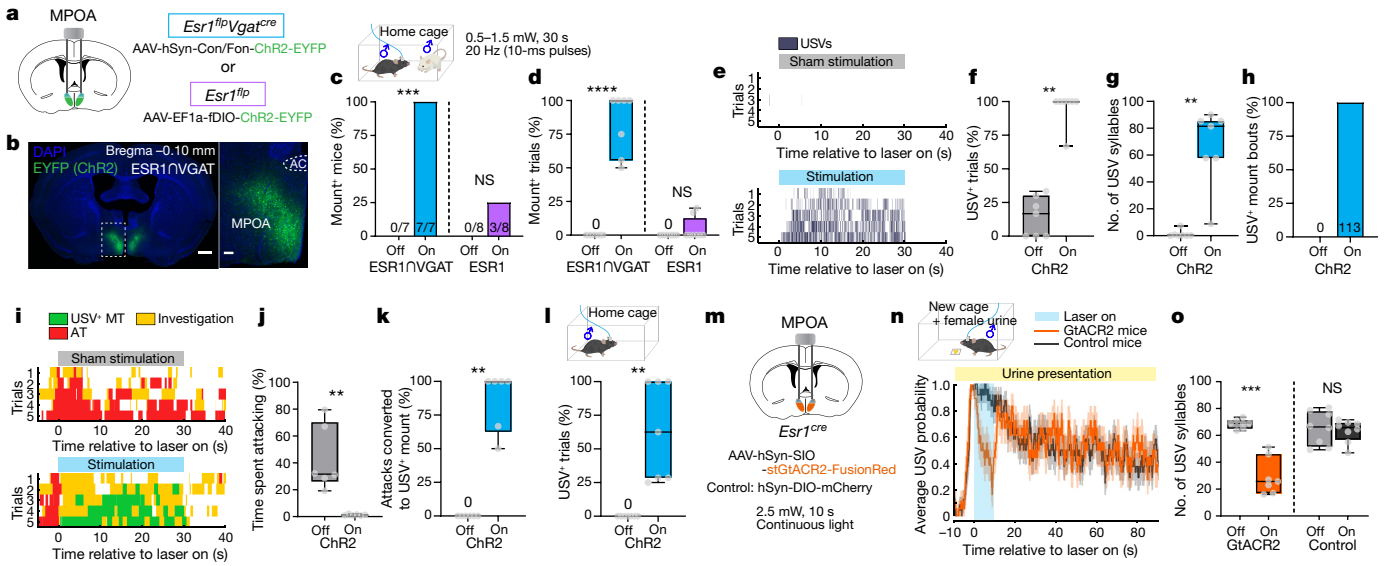

Fig. 3 | MPOA$^{ESR1\cap VGAT}$ neurons control male sexual behaviour. a, Strategy to express ChR2 in MPOA$^{ESR1\cap VGAT}$ or MPOA^{ESR1} neurons using sexually and socially experienced *Esr1^{flp} Vgat^{cre}* (blue bars) or *Esr1^{flp}* (purple bars) mice. Con/Fon, Cre-ON/FLP-ON; fDIO, FLP-ON. **b**, ChR2 expression in MPOA in *Esr1^{flp} Vgat^{cre}* mice with boxed region magnified (right). Scale bars, 500 µm (left), 100 µm (right). $n = 7$. **c**, **d**, Optogenetically triggered mounting towards male intruders. **c**, Fraction of mice mounting. NS, not significant; $^{***}P = 0.0006$. **d**, Fraction of photostimulation trials with mounting. $^{****}P < 0.0001$. MPOA$^{ESR1\cap VGAT}$, $n = 7$; MPOA^{ESR1}, $n = 8$. Off, sham photostimulation; On, during photostimulation (Extended Data Fig. 7). **e**–**g**, ChR2-triggered USVs with male intruder. **e**, USV raster plots. **f**, Fraction of trials with USVs. **g**, Number of USV syllables per trial. $n = 7$. **f**, $^{**}P = 0.0012$; **g**, $^{**}P = 0.0025$. **h**, Per cent of mount bouts that were USV^{+} during photostimulation. Numbers indicate total mounts (USV^{+} and USV^{-}) observed. **i**–**k**, Photostimulation of MPOA$^{ESR1\cap VGAT}$ neurons initiated during attack towards male intruder. **i**, Behaviour raster plots. **j**, Fraction of total time spent attacking. **k**, Fraction of attacks converted to USV^{+} mounts. $n = 6$. **j**, $^{**}P = 0.0027$; **k**, $^{**}P = 0.0014$. **l**–**o**, Solitary male mice. **l**, Fraction of USV^{+} trials in solitary male mice during photostimulation. $n = 7$. $^{**}P = 0.0045$. **m**, Strategy to optogenetically inhibit[29] MPOA^{ESR1} neurons in male *Esr1^{cre}* mice. **n**, **o**, Female-urine-evoked USVs during MPOA^{ESR1} photoinhibition (pale blue bar). **n**, Probability of USVs. GtACR2 mice, mice injected with GtACR2-coding AAV; control mice, mice injected with mCherry-coding AAV. **o**, Number of USV syllables. Orange, GtACR2, $n = 7$; grey, control, $n = 8$, $^{***}P = 0.0008$. Qualitatively similar results were obtained with iC++ inhibition of MPOA$^{ESR1\cap VGAT}$ neurons. **c**, Fisher's test; **d**, **f**, **g**, **j**–**l**, **o**, Kruskal–Wallis test. Data are mean ± s.e.m. except for box plots (see Fig. 2 legend for box plot definitions). All statistical tests are two-sided and corrected for multiple comparisons when necessary (Supplementary Table 2).

(coloured points in Fig. 2o, p, s, t). Accordingly, linear decoders—a type of binary classifier based on a support vector machine learning algorithm—could be trained to distinguish these two types of mounting on the basis of the pattern of neuronal activity in both nuclei, with 70–80% accuracy (Fig. 2q, r, u, v, Methods). Nevertheless, decoder performance may reflect the encoding of the sex of the intruder as well as of mount type, because the two are highly correlated.

We next investigated the respective causal roles of the MPOA and VMHvl in sexual and aggressive mounting. Although male mounting is promoted by electrical stimulation of the MPOA[19,20], we observed only weak and inefficient promotion of mounting by activating MPOA^{ESR1} neurons (purple bars in Fig. 3c, d), confirming a previous study[8]. Because MPOA^{ESR1} neurons comprise a mixture of approximately 80% GABAergic and approximately 20% glutamatergic neurons[8,21] and because mating-induced *Fos* expression is stronger in preoptic inhibitory than in excitatory neurons[15], we reasoned that intersectionally targeting ESR1^{+} GABAergic neurons might enrich for MPOA neurons that promote male sexual behaviour.

Indeed, intersectional optogenetic activation[22] of MPOA$^{ESR1\cap VGAT}$ neurons using *Esr1^{flp} Vgat^{cre}* (*Vgat* is also known as *Slc32a1*) mice (Fig. 3a, b) robustly and efficiently promoted investigation and mounting of a male intruder, at stimulation intensities over an order of magnitude lower (0.5–1.5 mW) than those previously reported using *Esr1^{cre}* mice[8] (blue in Fig. 3c, d, Extended Data Fig. 7a–c, Supplementary Video 3). Importantly, stimulation of MPOA$^{ESR1\cap VGAT}$ neurons evoked USV^{+} mounting towards both male and female intruders (Fig. 3e–h, Extended Data Fig. 7a–c, j–m), as well as towards some inanimate objects (Supplementary Video 4). Optogenetic stimulation also elicited USVs in solitary male mice[23] (Fig. 3l, Extended Data Fig. 7i), which confirms that vocalizations were not secondary to mounting or emitted by intruders. Optogenetically evoked USVs exhibited similar syllable patterns and acoustic features to those emitted naturally by male mice exposed to female mice[2–4,23,24] or to female urine[25] (Extended Data Fig. 8). Notably, activation of MPOA$^{ESR1\cap VGAT}$ neurons also rapidly interrupted ongoing attack, and converted it to male-directed USV^{+} mounting (Fig. 3i–k, Extended Data Fig. 7f, g, Supplementary Video 5). Furthermore, activation of MPOA$^{ESR1\cap VGAT}$ neurons in female mice evoked male-typical USV^{+} mounting behaviour towards male mice[8] and inanimate objects (Supplementary Video 6). Thus, activation of MPOA$^{ESR1\cap VGAT}$ neurons triggered a programme of male-typical mounting behaviour in both male and female mice, independent of target identity. The silencing of MPOA^{ESR1} neurons[8] attenuated USVs evoked by female urine in solitary male mice[25] (Fig. 3m–o), which indicates that these neurons are necessary for such vocalizations—as well as for mounting, as previously reported[8] and confirmed here (Extended Data Fig. 9a–e).

Weak optogenetic stimulation of VMHvl^{ESR1} neurons is known to promote mounting, whereas strong stimulation promotes attack[12]. However, it was not clear whether such mounting is sexual (USV^{+}) or aggressive (USV^{-}). Audio recordings indicated that weak VMHvl^{ESR1} activation promoted USV^{-} mounting towards both female and castrated male intruders, as well as attack (Fig. 4a–k, Extended Data Fig. 10b–d, f–i). These results suggest that mounting evoked by the activation of VMHvl^{ESR1} neurons represents a low-intensity form of aggression. Nevertheless, the silencing of VMHvl^{ESR1} neurons strongly suppressed spontaneous female-directed (sexual) mounting (Extended Data Fig. 9j–m), confirming and extending previous reports of weak inhibitory effects[9–11]. These differential effects of gain- versus loss-of-function manipulations of VMHvl^{ESR1} neurons on USV^{+} versus USV^{-} mounting probably reflect influences on distinct female- and male-responsive subpopulations[6,16,26] (Extended Data Fig. 10q, Supplementary Note 3).

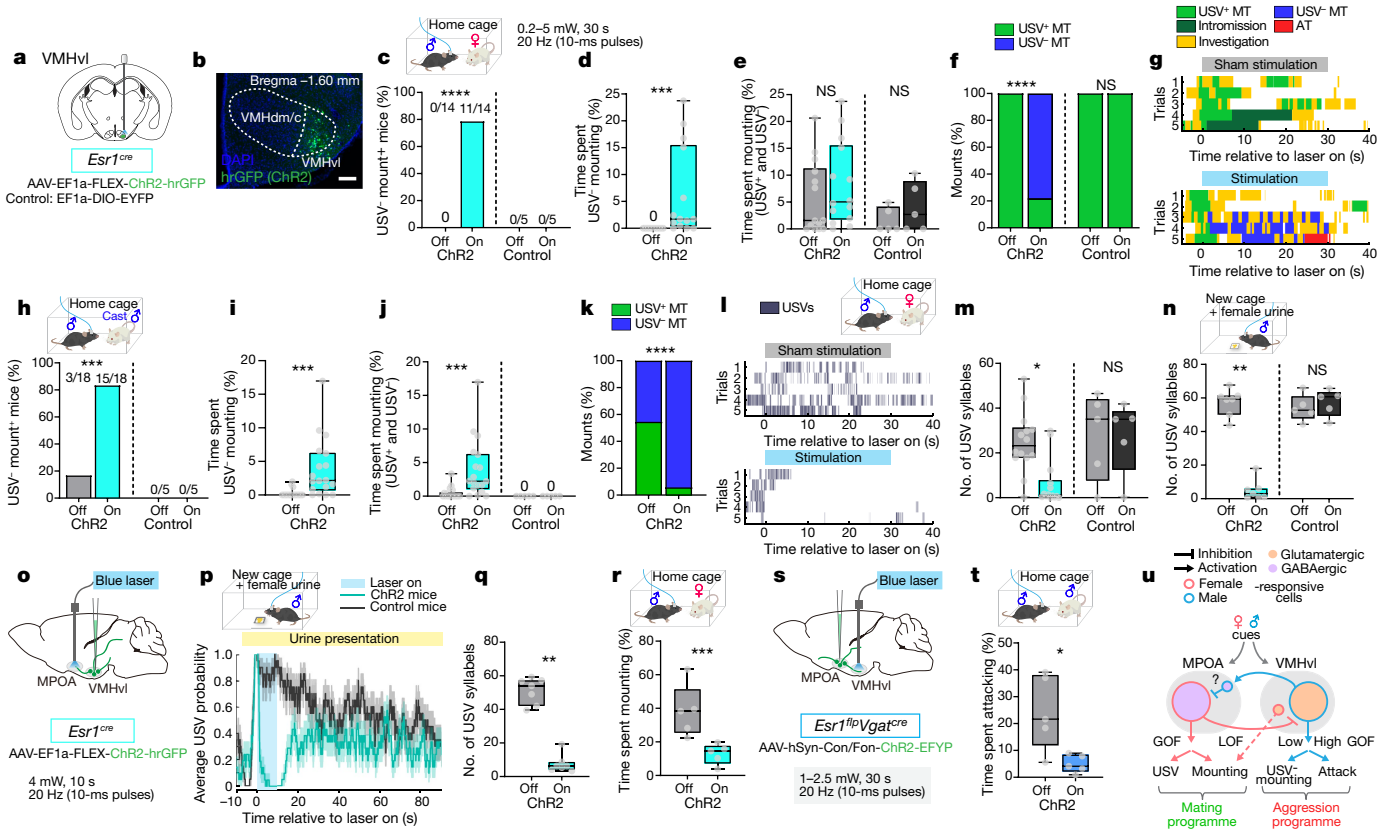

Fig. 4 | VMHvl^{ESR1} neurons promote aggressive mounting and inhibit USV production. a, Strategy to optogenetically activate VMHvl^{ESR1} neurons in naive male mice. **b**, ChR2 expression in VMHvl. Scale bar, 100 µm. $n = 18$. VMHdm/c, dorsomedial and central parts of the VMH. **c**–**g**, Behaviours towards female intruders during photostimulation. ChR2 mice, mice injected with ChR2-coding AAV; control mice, mice injected with EYFP-coding AAV. ChR2, $n = 14$; control, $n = 5$. **c**, Fraction of mice displaying USV$^-$ mounting. $^{****}P < 0.0001$. **d**, Per cent time spent USV$^-$ mounting. $^{***}P = 0.001$. **e**, Per cent time spent in all mounting. **f**, Fraction of USV$^+$ and USV$^-$ mounts. $^{****}P < 0.0001$. **g**, Behaviour raster plots. **h**–**k**, Behaviours towards castrated male intruders. ChR2, $n = 18$; control, $n = 6$. **h**, Fraction of mice displaying USV$^-$ mounting. **i**, Per cent time spent USV$^-$ mounting. $^{***}P = 0.0003$. **j**, Per cent time spent in all mounting. $^{***}P = 0.0002$. **k**, Fraction of USV$^+$ and USV$^-$ mounts. $^{****}P < 0.0001$. **l**, **m**, Spontaneous USVs towards female intruder during VMHvl^{ESR1} photostimulation. **l**, USV raster plots. **m**, Number of USV syllables. ChR2, $n = 14$; control, $n = 5$. $^{*}P = 0.01$. **n**, Female-urine-evoked USVs in solitary male mouse during photostimulation. ChR2, $n = 14$; control, $n = 7$. $^{**}P = 0.002$. **o**, Strategy to optogenetically activate ESR1$^{VMHvl \rightarrow MPOA}$ axon terminals. **p**–**r**, Female-urine-evoked USVs and mounting during terminal stimulation. **p**, Probability of USVs. **q**, Number of USV syllables. ChR2, $n = 7$; control, $n = 7$, $^{**}P = 0.0065$. **r**, Per cent time spent mounting during photostimulation, triggered after mount onset. ChR2, $n = 5$, $^{***}P = 0.0006$. **s**, Strategy to optogenetically activate ESR1∩VGAT$^{MPOA \rightarrow VMHvl}$ axon terminals. **t**, Per cent time spent attacking during photostimulation, triggered after attack onset. ChR2, $n = 5$, $^{*}P = 0.034$. **u**, Summary of perturbation effects. GOF, gain-of-function effect; LOF, loss-of-function effect only; low and high denote relative stimulation intensities in optogenetic gain-of-function experiments[12]. Function of minor cell populations (small circles) is hypothetical. More details are provided in Extended Data Fig. 10q, Supplementary Note 3. **c**, **f**, **h**, **k**, Fisher's test. **d**, **i**, Wilcoxon test. **e**, **j**, **m**, **n**, **q**, **r**, **t**, Kruskal–Wallis test. Data are mean ± s.e.m., except for box plots (see Fig. 2 legend for definitions). All statistical tests are two-sided and corrected for multiple comparisons when necessary (Supplementary Table 2).

Importantly, VMHvl^{ESR1} stimulation did not simply fail to evoke USVs, but instead strongly inhibited the USVs elicited by female intruders or urine (Fig. 4l–n). We therefore asked where it is that this inhibitory effect is exerted. VMHvl^{ESR1} neurons project strongly to the MPOA[27]. Optogenetic stimulation of VMHvl^{ESR1} terminals in the MPOA strongly inhibited female-urine-evoked USVs[25] (Fig. 4o–q), as well as female-directed mounting (Fig. 4r). As VMHvl^{ESR1} neurons are largely excitatory[16,26], this inhibitory effect may occur indirectly via local interneurons in the MPOA (Fig. 4u, Extended Data Fig. 10q, Supplementary Note 3). However, we cannot exclude the activation of collateral targets[27] via back-propagation of spikes. Conversely, optogenetic stimulation of MPOA$^{ESR1 \cap VGAT}$ terminals in VMHvl strongly inhibited aggression (Fig. 4 s, t). Thus, activation of MPOA-projecting VMHvl^{ESR1} (ESR1$^{VMHvl \rightarrow MPOA}$) and VMHvl-projecting MPOA$^{ESR1 \cap VGAT}$ (ESR1∩VGAT$^{MPOA \rightarrow VMHvl}$) neurons suppressed female-directed mounting and male-directed aggression, respectively, implying a reciprocal inhibitory circuit motif as previously suggested[28] (Fig. 4u).

We have investigated how same- and opposite-sex-directed male mounting is controlled in the hypothalamus. We find that these two forms of mounting are distinct behaviours that are controlled by different hypothalamic cell populations. Imaging experiments in each nucleus revealed relatively rare populations of USV$^+$- or USV$^-$-mount-selective cells; most MPOA^{ESR1} and VMHvl^{ESR1} neurons exhibited mixed selectivity for multiple social behaviours towards an intruder of a given sex. These data suggest that these two major populations principally control reproductive and aggressive states, respectively, which explains the causally dominant behavioural effects of optogenetic stimulation. Nevertheless, the MPOA—as with the VMHvl[6,16,26]—also contains a minor subpopulation of neurons (about 9%) (Fig. 2g) that is selectively activated during the opposing state. In the case of the VMHvl, it seems likely that the female-preferring cells are required for mating behaviour[9,10] (Extended Data Figs. 9l, m, 10q, Supplementary Note 3). In the case of the MPOA, the male-preferring ESR1$^+$ subpopulation could either indirectly promote aggression or suppress mounting during fighting. Whatever the case, our data suggest that aggressive and reproductive (sexual) states are represented by heterogeneous cell populations distributed across multiple

hypothalamic nuclei. More generally, they show that a superficially similar motor action can be controlled by distinct neural subpopulations that encode opposing motivational states, at the level of the hypothalamus.

Online content

Any methods, additional references, Nature Research reporting summaries, source data, extended data, supplementary information, acknowledgements, peer review information; details of author contributions and competing interests; and statements of data and code availability are available at https://doi.org/10.1038/s41586-020-2995-0.

1. Bailey, N. W. & Zuk, M. Same-sex sexual behavior and evolution. *Trends Ecol. Evol.* **24**, 439–446 (2009).
2. Nyby, J. Ultrasonic vocalizations during sex behavior of male house mice (*Mus musculus*): a description. *Behav. Neural Biol.* **39**, 128–134 (1983).
3. White, N. R., Prasad, M., Barfield, R. J. & Nyby, J. G. 40- and 70-kHz vocalizations of mice (*Mus musculus*) during copulation. *Physiol. Behav.* **63**, 467–473 (1998).
4. Holy, T. E. & Guo, Z. Ultrasonic songs of male mice. *PLoS Biol.* **3**, e386 (2005).
5. Segalin, C. et al. The mouse action recognition system (MARS): a software pipeline for automated analysis of social behaviors in mice. Preprint at https://doi.org/10.1101/2020.07.26.222299 (2020).
6. Remedios, R. et al. Social behaviour shapes hypothalamic neural ensemble representations of conspecific sex. *Nature* **550**, 388–392 (2017).
7. Stagkourakis, S. et al. A neural network for intermale aggression to establish social hierarchy. *Nat. Neurosci.* **21**, 834–842 (2018).
8. Wei, Y. C. et al. Medial preoptic area in mice is capable of mediating sexually dimorphic behaviors regardless of gender. *Nat. Commun.* **9**, 279 (2018).
9. Sano, K., Tsuda, M. C., Musatov, S., Sakamoto, T. & Ogawa, S. Differential effects of site-specific knockdown of estrogen receptor α in the medial amygdala, medial pre-optic area, and ventromedial nucleus of the hypothalamus on sexual and aggressive behavior of male mice. *Eur. J. Neurosci.* **37**, 1308–1319 (2013).
10. Yang, C. F. et al. Sexually dimorphic neurons in the ventromedial hypothalamus govern mating in both sexes and aggression in males. *Cell* **153**, 896–909 (2013).
11. Yang, T. et al. Social control of hypothalamus-mediated male aggression. *Neuron* **95**, 955–970 (2017).
12. Lee, H. et al. Scalable control of mounting and attack by Esr1^{+} neurons in the ventromedial hypothalamus. *Nature* **509**, 627–632 (2014).
13. Lerner, T. N. et al. Intact-brain analyses reveal distinct information carried by SNc dopamine subcircuits. *Cell* **162**, 635–647 (2015).
14. Stowers, L., Holy, T. E., Meister, M., Dulac, C. & Koentges, G. Loss of sex discrimination and male–male aggression in mice deficient for TRP2. *Science* **295**, 1493–1500 (2002).
15. Moffitt, J. R. et al. Molecular, spatial, and functional single-cell profiling of the hypothalamic preoptic region. *Science* **362**, eaau5324 (2018).
16. Kim, D. W. et al. Multimodal analysis of cell types in a hypothalamic node controlling social behavior. *Cell* **179**, 713–728 (2019).
17. Ziv, Y. et al. Long-term dynamics of CA1 hippocampal place codes. *Nat. Neurosci.* **16**, 264–266 (2013).
18. Shadlen, M. N., Britten, K. H., Newsome, W. T. & Movshon, J. A. A computational analysis of the relationship between neuronal and behavioral responses to visual motion. *J. Neurosci.* **16**, 1486–1510 (1996).
19. Malsbury, C. W. Facilitation of male rat copulatory behavior by electrical stimulation of the medial preoptic area. *Physiol. Behav.* **7**, 797–805 (1971).
20. Vaughan, E. & Fisher, A. E. Male sexual behavior induced by intracranial electrical stimulation. *Science* **137**, 758–760 (1962).
21. Hahn, J. D., Sporns, O., Watts, A. G. & Swanson, L. W. Macroscale intrinsic network architecture of the hypothalamus. *Proc. Natl Acad. Sci. USA* **116**, 8018–8027 (2019).
22. Fenno, L. E. et al. Targeting cells with single vectors using multiple-feature Boolean logic. *Nat. Methods* **11**, 763–772 (2014).
23. Gao, S.-C., Wei, Y.-C., Wang, S.-R. & Xu, X.-H. Medial preoptic area modulates courtship ultrasonic vocalization in adult male mice. *Neurosci. Bull.* **35**, 697–708 (2019).
24. Tschida, K. et al. A specialized neural circuit gates social vocalizations in the mouse. *Neuron* **103**, 459–472 (2019).
25. Nyby, J., Wysocki, C. J., Whitney, G., Dizinno, G. & Schneider, J. Elicitation of male mouse (*Mus musculus*) ultrasonic vocalizations. 1. Urinary cues. *J. Comp. Physiol. Psychol.* **93**, 957–975 (1979).
26. Lin, D. et al. Functional identification of an aggression locus in the mouse hypothalamus. *Nature* **470**, 221–226 (2011).
27. Lo, L. et al. Connectional architecture of a mouse hypothalamic circuit node controlling social behavior. *Proc. Natl Acad. Sci. USA* **116**, 7503–7512 (2019).
28. Tinbergen, N. *The Study of Instinct* (Clarendon/Oxford Univ. Press, 1951).
29. Mahn, M. et al. High-efficiency optogenetic silencing with soma-targeted anion-conducting channelrhodopsins. *Nat. Commun.* **9**, 4125 (2018).

Methods

No statistical methods were used to predetermine sample size. The order of male or female intruder experiments were performed in the random order in imaging experiments, but were not randomized in functional manipulation experiments. Investigators were blind to experimental or control groups during functional manipulation experiments and outcome assessment.

Mice

All experimental procedures involving the use of live mice or their tissues were carried out in accordance with NIH guidelines and approved by the Institute Animal Care and Use Committee (IACUC) and the Institute Biosafety Committee (IBC) at the California Institute of Technology (Caltech). All C57BL/6N mice used in this study, including wild-type and transgenic mice, were bred at Caltech. BALB/c male and female mice were used as intruder mice and bred at Caltech or purchased from Charles River Laboratories (CRL). BALB/c ovariectomized female mice and castrated male mice were purchased from CRL. Experimental mice were used at the age of 2–4 months. Intruder mice were used at the age of 2–6 months and were maintained with three to five cage mates to reduce their aggression. *Esr1*^{cre} knock-in mice[12] (Jackson Laboratory stock no. 017911), *Esr1*^{flp} knock-in mice (described in 'Generation of *Esr1*^{flp} knock-in mice') and *Slc32a1* (*Vgat*)^{cre} knock-in mice[30] (Jackson Laboratory stock no. 028862) were backcrossed into the C57BL/6N background (>N10) and bred at Caltech. Heterozygous *Esr1*^{cre}, *Esr1*^{flp} or double heterozygotes *Esr1*^{flp} *Vgat*^{cre} mice were used for cell-specific targeting experiments, and were genotyped by PCR analysis using genomic DNA from tail or ear tissue. All mice were housed in ventilated micro-isolator cages in a temperature-controlled environment (median temperature 23 °C, humidity 60%), under a reversed 11-h dark–13-h light cycle, with ad libitum access to food and water. Mouse cages were changed weekly.

Generation of *Esr1*^{flp} knock-in mice

Esr1^{flp} knock-in mice were generated at the Caltech Genetically Engineered Mouse Services core facility, following standard procedures. The targeting vector was designed in the same way as *Esr1*^{cre} [12]. Instead of Cre recombinase, an F2A sequence and a Flp recombinase[31] coding sequence were inserted at the 3′ end of the *Esr1* coding sequence, by in-frame homologous recombination. Following electroporation of the targeting construct into 129S6/SvEvTac-derived TC-1 embryonic stem cells, correctly targeted cells were identified by PCR genotyping using the following primer sets: 5′ arm primers (6.7 kb), 5′-cccatggccactagacactt-3′ and 5′-acgtctccgcatgtcagaag-3′; 3′ arm primers (4 kb), 5′-taagggatatttgcctggccc -3′ and 5′-ctcgacgaccaatgacctct -3′. Positive embryonic stem cells were injected into recipient C57BL/6N blastocysts to generate chimeric males that were then bred with C57BL/6N female mice. Mouse genotype was determined by PCR using genomic DNA templates isolated from tail or ear tissue with the following primer sets: wild-type allele (0.6 kb) 5′-tggccactcatactagaaagccactg-3′ and 5′-ggaggaaatgaaaatacgtggacacaagtccc-3′; targeted allele (1 kb) 5′-ttgtgccccctctatgacctgctc -3′ and 5′- gggtccacgttcttgatgtcgct -3′.

Hormone treatment

To enhance the sexual receptivity of female mice, hormone primed BALB/c female mice were used as intruders in some experiments (Figs. 1, 4r, Extended Data Fig. 9c–f, l–o). Ovariectomized female mice received subcutaneous injections of 10 μg of β-oestradiol-3-benzoate (E8515, Sigma-Aldrich) in sesame oil (S3547, Sigma-Aldrich) at 48 h, and 500 μg progesterone (P0130, Sigma-Aldrich) at 4–6 h before behavioural experiments[32].

Surgery

Surgeries were performed on adult *Esr1*^{cre}, *Esr1*^{flp} or *Esr1*^{flp}*Vgat*^{cre} mice aged 8–12 weeks. Virus injection and implantation were performed as previously described[26]. In brief, mice were anaesthetized with isoflurane (0.8–5%) and placed on a stereotaxic frame (David Kopf Instruments). Then, 100–200 nl of virus was injected into the target area using a pulled glass capillary (World Precision Instruments) and a pressure injector (Micro4 controller, World Precision Instruments), at a flow rate of 20–50 nl min^{-1}. Typically, the injection volumes were 200 nl for MPOA and 100 nl for VMHvl. For GCaMP viruses, the injection volumes were 150 nl for fibre photometry experiments and 200 nl for micro-endoscope experiments, for both MPOA and VMHvl. Stereotaxic injection coordinates were based on the Paxinos and Franklin atlas[33] (MPOA, anterior–posterior: −0.1, medial–lateral: ±0.45, dorsal–ventral: −4.75; VMHvl, anterior–posterior: −1.5, medial–lateral: ±0.75, dorsal–ventral: −5.73). For optogenetic and fibre photometry experiments, single or dual optic fibres (optogenetics: diameter 200 μm, N.A., 0.22; fibre photometry: diameter 400 μm, N.A., 0.48; Doric lenses) were subsequently placed 250–300 μm above the virus injection sites and fixed on the skull with dental cement (Parkell). Mice were allowed to recover for at least two weeks before behavioural testing. For micro-endoscope experiments, virus injection and lens implantation were performed either on the same day, or one to two weeks apart, respectively. GRIN lenses (Inscoipix, diameter 0.6 × 7.3 or 1 × 9 mm) were slowly lowered into the brain without a cannula, and fixed to the skull with dental cement (Parkell). Mice were initially checked for epifluorescence signals three to four weeks after virus injection. To perform such checks, mice were either anaesthetized with isoflurane and mounted on a stereotaxic frame, or head-fixed and placed on a running wheel while awake. A head-mounted miniaturized micro-endoscope (nVista2 or nVista3, Inscopix) was then lowered over the implanted lens until GCaMP-expressing fluorescent neurons were in focus. If fluorescent neurons were not observed, the mice were returned to their cages and checked again on a weekly basis. If GCaMP-expressing neurons were detected, the micro-endoscope was aligned and a permanent baseplate was attached to the head with dental cement, as previously described[34]. To habituate mice to the weight of the micro-endoscope, a weight-matched dummy micro-endoscope (Inscopix) was attached to the baseplate, and the mice were allowed to recover for at least a week before behavioural testing.

Virus

The following AAVs were used in this study, with injection titres as indicated. When the original viral titre was high, AAVs were diluted with clean PBS on the day of use. AAV2-hSyn-DIO-hm4D-mCherry (3.7×10^{12} genome copies per ml), AAVDJ-hSyn-Con/Fon-hChR2(H134R)-EYFP (2.2×10^{12}), AAVDJ-hSyn-Con/Fon-EYFP (2.5×10^{12}) AAV2-EF1a-DIO-hChR2(H134R)-EYFP (2×10^{12}), AAV5-EF1a-DIO-EYFP (3.2×10^{12}), AAVDJ-EF1a-fDIO-hChR2(H134R)-EYFP (2×10^{12}) and AAVDJ-EF1a-fDIO-EYFP (2.1×10^{12}) were purchased from the UNC vector core. AAV1-hSyn-Flex-GCaMP6 s (5×10^{12} for fibre photometry and 1×10^{12} for micro-endoscope imaging) was purchased from the U. Penn Vector Core. AAV2-hSyn-DIO-mCherry (2.5×10^{12}) was purchased from Addgene. AAVDJ-hSyn-SIO-stGtACR2-FusionRed (5.4×10^{12}, Addgene plasmid no. 105677), and AAV2-EF1a-Flex-hChR2-V5-F2A-hrGFP[12] (1.95×10^{12}) were packaged at the HHMI Janelia Research Campus virus facility.

Histology

Following completion of behavioural experiments, histological verification of virus expression and implant placement were performed on all mice. Mice lacking correct virus expression or implant placement were excluded from the analysis. In brief, mice were perfused transcardially with 0.9% saline at room temperature, followed by 4% paraformaldehyde (PFA) in 1× PBS. Brains were extracted and post-fixed in 4% PFA overnight at 4 °C, followed by 24 h in 30% sucrose/PBS at 4 °C. Brains were embedded in OCT mounting medium, frozen on dry ice and stored at −80 °C for subsequent sectioning. Brains were sectioned in 50–75-μm thickness on a cryostat (Leica Biosystems). Sections were washed with 1× PBS and mounted on Superfrost slides, then incubated for 30 min at

room temperature in DAPI/PBS (0.5 μg/ml) for counterstaining, washed again and coverslipped. Sections were imaged with epifluorescent microscope (Olympus VS120).

Behavioural tests

Sexual and social experience and housing conditions. For the experiment in Fig. 1, 8–12-week-old C57BL/6N male mice were individually cohoused with a BALB/c female mice for a week, and female mice were removed from the cages one day before the experiments. Hormone-primed BALB/c female mice or intact BALB/c male mice were used as intruders. For all optogenetic (except VMHvl cell body optogenetic stimulation; Fig. 4a–m), fibre photometry, micro-endoscope and chemogenetic experiments, transgenic mice were first separated from siblings and cohoused with C57BL/6N or BALB/c female mice for a week, then introduced to several BALB/c male intruders for 15 min for 3 consecutive days, to give them aggression experience. After sexual and social experience, male mice were always cohoused with female mice. If female mice became pregnant during the cohousing, new female mice were provided as cage mates. For VMHvl cell body optogenetic stimulation with intruder mice (Fig. 4a–m, Extended Data Fig. 10a–d,f–i), male mice were not sexually and socially experienced to avoid the development of excessive aggressiveness[12,35]. Male mice were separated from siblings on the day of surgery and then maintained under single-housing conditions. Castrated male mice were used as intruders to reduce baseline aggression of resident mice. Following the completion of testing with castrated male and female intruders, resident mice were cohoused with female mice for a week and then tested with female urine (Fig. 4n, Extended Data Fig. 10e) to evoke USVs.

Behaviour and audio recording. All behavioural experiments were performed in conventional mouse housing cages (home cage or new cage) under red lighting, using the previously described behaviour recording setup[36]. Both top and front views of the behaviour videos were acquired at 30 Hz using video recording software, StreamPix7 (Norpix). Audio recordings were collected at a 300-kHz sampling rate using an Avisoft-UltraSoundGate 116H kit with a condenser ultrasound microphone CM16/CMPA (Avisoft-Bioacoustics), positioned 45 cm above the arena. Initiation of audio recording was synchronized with video recording via a signal generated by StreamPix7.

Resident–intruder test. Mouse cages were not cleaned for a minimum of three days before the behavioural test, to retain the odours of the resident mouse. Resident mice were introduced to the behaviour recording setup in their home cage, and allowed to rest for at least five minutes before starting behaviour tests. For the experiments in Fig. 1, Extended Data Fig. 9c–f, l–o, resident mice were allowed to interact with female intruders for 15 min. For Fig. 1, resident mice were allowed to interact with male intruders for 20 min. When an excessive amount of aggression was observed, tests were terminated at 10 min. For Extended Data Fig. 9g–i, resident mice were allowed to interact with male intruders for 10 min. Behaviour tests were performed during the subjective dark period of the mouse housing room day–night cycle (from 2–8 h after lights off).

Optogenetic stimulation and inhibition. Before initiating behavioural experiments, the light intensity achieved at the tip of the optic fibre was estimated by connecting an equivalent optic fibre to the patch cable, and measuring the light intensity at the tip of the fibre using a power meter. Laser power was controlled by turning an analogue knob on the laser power supply. Mice were connected to a 473-nm or 455-nm laser (Shanghai Laser and Optics Century or Changchun New Industries Optoelectronics Tech) via optical patch cords (diameter 200 μm, N.A., 0.22, Doric lenses and Thorlabs) and a rotary joint (Doric lenses). Mice were allowed to habituate to the cables after connecting them for at least 5 min before starting behaviour tests. The experimenter monitored mouse behaviour via a computer monitor in a room adjacent to the behavioural arena, and triggered the laser manually when animals were engaged in the behaviours of interest. Sham stimulation (laser off) was interleaved with the light stimulation (laser on) as an internal control. For optogenetic stimulation, mice were given trains of photostimulation (10-ms pulse, 20 Hz for 10 or 30 s), with at least a three-minute interval between trains. For optogenetic inhibition, 10 s of continuous photostimulation was used. The frequency and duration of photostimulation were controlled using an Accupulse Generator (World Precision Instruments) or an Isolated Pulse Stimulator (A-M Systems).

Urine presentation with optogenetic manipulation. For urine presentation experiments (Figs. 3m–o, 4n, p, q, Extended Data Fig. 10e, k, l), subject male mice were introduced into a new cage and allowed to explore for at least five minutes before testing. Group-housed C57BL/6N female mice were used as urine donors. Just before testing, the female mouse was lifted by the cervical region and her genital area was gently wiped with a small piece of nestlet (compressed cotton fibre nesting material), to absorb urine seeping from the ano-genital region. The urine-soaked nestlet was placed in the centre of the cage with the male mouse for two minutes, and then removed from the cage. Urine was presented to each male subject mouse approximately six times, with at least a three-minute interval between presentations. Urine from different female donors was used every time. The experimenter monitored the behaviour and vocalizations of the mice through a computer monitor, and delivered 10-s optogenetic stimulation or inhibition pulses at one to two seconds after the first USV syllable was detected. Light stimulation (laser on) and sham stimulation (laser off, same time period) trials were alternated.

Chemogenetic inhibition. Mice were injected with hM4Di-DREADD-mCherry or mCherry (control)-expressing AAVs in MPOA or VMHvl. Behavioural tests were performed on two consecutive days. The number of mice receiving saline or clozapine-*N*-oxide (CNO) (Enzo Life Sciences) was counterbalanced across the two days. CNO was dissolved in saline. CNO (7.5 mg/kg) or saline (control) was intraperitoneally injected 60 min before behavioural tests.

Dual-site fibre photometry recording. The fibre photometry setup was constructed as previously described[13] with minor modifications. We prepared two sets of light paths (ch1 and ch2, recorded signals were processed by a common real-time processor) to enable measurement of bulk calcium signals in two brain regions simultaneously. MPOA and VMHvl recordings were assigned to ch1 or ch2 randomly. We used 470-nm LEDs (M470F3, Thorlabs, filtered with 470-10-nm bandpass filters FB470-10, Thorlabs) for fluorophore excitation, and 405-nm LEDs for isosbestic excitation (M405FP1, Thorlabs, filtered with 410–10-nm bandpass filters FB410-10, Thorlabs). LEDs were modulated at 208 Hz (470 nm) and 333 Hz (405 nm) for ch1, and 263 Hz (470 nm) and 481 Hz (405 nm) for ch2, and controlled by a real-time processor (RZ5P, Tucker David Technologies) via an LED driver (DC4104, Thorlabs). The emission signal from the isosbestic excitation was used as a reference to control for motion artefacts and photobleaching[13,37]. LEDs were coupled to a 425-nm longpass dichroic mirror (Thorlabs, DMLP425R) via fibre optic patch cables (diameter 400 μm, N.A., 0.48; Doric lenses). Emitted light was collected via the patch cable, coupled to a 490-nm longpass dichroic mirror (DMLP490R, Thorlabs), filtered (FF01-542/27-25, Semrock), collimated through a focusing lens (F671SMA-405, Thorlabs) and detected by the photodetectors (Model 2151, Newport). Recordings were acquired using Synapse software (Tucker Davis Technologies). Once the patch cables were connected to the optic fibre implants on the head of the mice, the mice were placed in their home cage and allowed to habituate for at least 10 min before starting behavioural test sessions. Male or female intruders were introduced into the home cage in a random order, with a 5–10-min interval between male and

female intruder sessions. Typically, a session for encountering male or female intruders lasted 10–20 min. Because MPOA and VMHvl are highly interconnected[38,39], fluorescent signals from cells in one nucleus may be contaminated with afferent terminal signals derived from the other. As such interconnections are primarily ipsilateral (Extended Data Fig. 2c–f), and activity in a given nucleus is highly correlated across hemispheres (Extended Data Fig. 2g–i), we avoided this contamination by recoding signals from contralateral MPOA and VMHvl.

Micro-endoscope imaging. Mice were temporarily head-fixed on a running wheel before imaging sessions, and the head-mounted dummy scope used for habituation was replaced with a micro-endoscope (nVista2 or nVista3, Inscopix). The mice were placed in their home cages and allowed to habituate for at least 10 min before starting behavioural test sessions. Shortly before data acquisition, the imaging parameters were configured using nVista control software (Inscopix). The field of view was cropped to the region encompassing the fluorescent neurons. Ca^{2+} imaging data were acquired at 15 Hz, 15–20% LED power and 2–3× gain, depending on the brightness of GCaMP expression. A TTL pulse from the sync port of the data acquisition box (DAQ, Inscopix) was used to synchronously trigger StreamPix7 for video recording, and Avisoft-UltraSoundGate for audio recording, via customized MATLAB scripts. Male or female intruders were introduced into the home cage in a random order, with a 5–10-min interval between male and female intruder sessions. Typically, a session for encountering male or female intruders lasted 10–20 min. MPOA and VMHvl imaging was performed in separate mice. Four GCaMP6s AAV-injected mice were used for $MPOA^{ESR1}$ (total of 583 neurons imaged) and $VMHvl^{ESR1}$ (total of 421 neurons imaged) for micro-endoscope imaging analysis, respectively.

Data analysis

Position tracking. Positions and poses of both resident and intruder mice were estimated on a frame-by-frame basis from top-view video using a Python-based custom deep neural network architecture developed in collaboration with the laboratory of P. Perona at Caltech (details of this system are available from ref. [5]). In brief, on each frame of video this system estimates the pose of each mouse in terms of the x–y coordinates of seven anatomically defined key points: the nose, the ears, the back of the neck, the hips and the base of the tail. The pose estimator was trained using manual annotations of anatomical key points in 13,500 frames sampled from 14 h of top-view videos of both unoperated mice and mice implanted with head-mounted cannulas or micro-endoscopes. All videos in the training set were of pairs of mice freely interacting in a standard home cage, and 1/3 of training data was taken from videos in which the resident mouse was implanted with a head-mounted micro-endoscope or fibre photometry device with attached cables. For the purposes of this study, the distance between mice was defined as the distance between the necks of the two mice, as estimated by the automated tracking software[5] ('tracker'). On held-out test data, 95% of neck key-point estimates by the tracker fell within a 0.44-cm radius of human-defined ground truth.

Behaviour annotation. Behaviour videos (collected at 30 Hz) were first processed using a custom automated behaviour classifier system[5] to generate frame-by-frame annotations of attack, mounting and investigation (sniffing) behaviour. Classifier output, videos and spectrograms of recorded audio were then loaded into a custom, MATLAB-based behaviour annotation interface[5], and classifier annotations were manually corrected by trained individuals blind to the experimental design, to produce a final set of frame-by-frame annotations of attack, USV^+ mounting, USV^- mounting, intromission and investigation (sniffing). Only one behavioural label was permitted per frame. USV^- mounting was operationally defined as bouts of mounting during which no USV syllables were detected (see 'USV detection'), in which we define a 'bout' of behaviour as a period of consecutive frames that all received positive annotations for that behaviour. In cases in which a USV^+ mount transitioned to a USV^- mount—for example, during optogenetic manipulation (Fig. 4c–k)—mounting bouts were annotated as USV^- mounts beginning 1 s after the last USV syllable. For scoring the latency to the first attack in Fig. 1n, the latency time for the mice that did not show attack within the testing period was calculated as 20 min.

Decoder analysis on behaviour features. We trained binary decoders to distinguish female- and male-directed mounting, on the basis of features extracted from videos of interacting mice. Fifty-four videos containing female- or male-directed interactions were annotated for USV^+ or USV^- mounting, on the basis of the presence or absence of USVs in audio recordings during mounting bouts, as outlined in 'Behaviour annotation'. From these, we extracted a total of 10,005 frames (>5.5 min) of female-directed USV^+ mounting across 162 behaviour bouts, and 7,527 frames (>4.1 min) of male-directed USV^- mounting across 185 behaviour bouts. We used a custom pose estimation system[5] to track seven key points on the bodies of both mice: the nose, ears, base of the neck, hips and the base of the tail. To classify behaviours, we extracted a set of 33 features computed from these pose key points, on the basis of features used in a previously published behaviour classification tool[36]. These features are defined in Supplementary Table 1. Importantly, features were purposefully selected to exclude measurements related to the size, movements and absolute position of the intruder mouse. This was a critical step, as otherwise our decoders were able to distinguish female- and male-directed mounting for 'trivial' reasons, such as the fact that intruder males were larger on average than intruder females, and the fact that intruder males tended to spend more time in the corner rather than the centre of the cage.

For frame-wise classification (Fig. 1b, c), the 33 features in Supplementary Table 1 were computed for each frame of USV^+ and USV^- mounting (at 30 Hz), and used to train a binary support vector machine (SVM) decoder for mounting type, with decoder performance evaluated using 'leave-one-out' cross-validation over the set of 54 behaviour videos. An equal number of USV^+ and USV^- mounting frames were sampled from each class to generate the training set. For classification based on temporal features (Extended Data Fig. 1e–g), the 33 features in Supplementary Table 1 were computed for every 5th frame (for video framerates of 30 Hz) from three seconds before to one second after the onset of USV^+ or USV^- mounting (25 time samples per feature per behaviour bout). All ($33 \times 25 = 825$) temporal features were then used to train a binary SVM decoder for mounting type, again using leave-one-out cross-validation across videos. To account for some jitter in the time-course of mount initiation, training and test frames were taken to be the annotated start of mounting, as well as all frames within a ±15-frame (500 ms) window of that start time.

USV detection. We created a spectrogram of recorded audio using the spectrogram function in MATLAB, with a 1024-point symmetric Hann window and 50% overlap between segments. To remove broad-spectrum background sound caused by the movements of mice in the homecage, we used a previously published multitapering and flattening approach[40] with time half-bandwidth product of six, to produce a cleaned spectrogram of the recorded audio. All spectrograms shown in the figures and videos are multitapered and flattened.

To detect USVs from the cleaned audio spectrograms, we used a supervised classifier (a multilayer perceptron) trained with manual annotations of USV syllables from 9 sample recordings totalling 17.3 min recording time, and including 1,663 syllables (26% of frames). As preprocessing before classification, spectrograms were cropped to the 30–125-kHz frequency range, z-scored and down-sampled by a factor of 0.5 in frequency space. To better capture temporal structure in the spectrogram, the mean and s.d. of each frequency bin was computed within a window of 8, 16 and 24 frames (approximately 14, 27 and 41 ms, respectively) around the current frame. Following USV

detection, all classifier output was manually validated in a custom MATLAB-based annotation interface[5], and false positives and false negatives were corrected.

There were several cases in which BALB/c male intruders emitted USVs during resident–intruder tests. Because C57BL/6N and BALB/c USVs differ in their acoustic features[41] (BALB/c USVs syllables are typically in a lower frequency range, and have a simpler structure), their USVs can often be visually distinguished in the spectrograms. When BALB/c USV syllables were clearly distinguishable from C57BL/6N USV syllables, they were removed from analysis. For the USV probability plots (Figs. 3n, 4p, Extended Data Fig. 10e, l), all the stimulation trials from all the tested mice were pooled and plotted with an s.e.m. envelope. USV probability traces were smoothed using a moving average with a 1-s time bin.

Fibre photometry data analysis. The fibre photometry recordings yielded two signals from each recording region, one at 405 nm (isosbestic Ca^{2+}-independent signal, for motion correction) and the other at 470 nm (Ca^{2+}-dependent signal). First, a least-squares linear fit was applied to the 405-nm signal from each region to align it to the 470-nm signal, yielding a fitted 405-nm signal. The motion-corrected 470-nm signal for each region was obtained as follows: motion-corrected 470-nm signal = (470-nm signal − fitted 405-nm signal)/fitted 405-nm signal. Next, to compare neural activity between MPOA and VMHvl, all the motion-corrected 470-nm traces obtained on a given experimental day from each region (always including both female and male intruder trials) were concatenated into a single trace. Concatenated traces from each region were then scaled from zero to one (scaled fluorescent traces, F_s), with pre-intruder activity (mean activity during 35 to 5 s before first intruder introduction, during which the mouse was in its home cage with no intruder present) set to zero and the maximum value of concatenated traces set to one. For computing peri-event time histograms (PETHs), $t = 0$ was set to the onset of a behaviour of interest (BOI), and the period from −5 to −3 s of the onset of the BOI was used as 'pre-behaviour baseline' period. We computed the mean (μ) and standard deviation (σ) of F_s over a pre-behaviour baseline period. PETH activity is computed as $\mathrm{PETH}(t) = (F_s(t) - \mu)/\sigma$. All PETH traces for a given BOI from each mouse were averaged and a single PETH trace was obtained from each individual mouse. PETH traces presented in the figures show the average across all the recorded mice, except for Extended Data Fig. 4, which shows the average across the BOI bouts from one mouse. Only behaviour bouts that were longer than 0.5 s, and separated by >5 s from the previous BOI bout, were used for PETH analysis. For computing maximum $\mathrm{activity}_{\mathrm{PETH}}$ (Extended Data Fig. 3b, e, g, j, n, r, v), mean values during the baseline period and the maximum value attained within the interval 0–3 s from the onset of the behaviour were compared. For calculating the area under the curve, the area under the Ca^{2+}-activity curve during the first BOI bout after $t = 0$ zero was calculated, and divided by the length of the first BOI bout to normalized to bout length. Because the first investigation bouts of each intruder have stronger prolonged calcium signals than all other investigation bouts in both MPOA and VMHvl, we excluded the period within 30 s from the beginning of first investigation from most of the analysis. First investigation bouts were analysed separately from other investigation bouts (Extended Data Fig. 3d, e, i, j).

Micro-endoscope trace extraction. Imaging frames were spatially downsampled by a factor of two in the x and y dimensions. Frames collected over the course of a single day (always including both female and male intruder trials) were concatenated into a single stack and registered to each other to correct for motion artefacts, using the Inscopix Data Processing software. To extract single cells and their Ca^{2+}-activity traces from the fluorescent imaging frames, we used the constrained non-negative matrix factorization for micro-endoscopic data (CNMF-E)[42] algorithm. CNMF-E outputs for putative individual neurons were individually inspected manually, and those that did not appear to correspond to single neurons were discarded.

Traces were normalized to units of σ with respect to the baseline fluorescence of the neuron before the first trial of resident–intruder interactions on a given day of imaging, as previously published[6]. In brief, for a given neuron with extracted calcium trace F_0(t), we computed the mean (μ) and standard deviation (σ) of $F_0(t)$ over a 'baseline' period of 30 or more seconds during which the mouse was in its home cage with no intruder present. Normalized calcium activity was then computed as $F(t) = (F_0(t) - \mu)/\sigma$.

Detection of sex-preferring neurons. In Fig. 2f, g, sex-preferring cells are defined as activated at least two s.d. from baseline by one but not the other sex during social interaction[6]. 'Other' includes neurons activated or inhibited by both or neither sexes.

Explained variance in micro-endoscope data. To calculate the variance in population neuronal activity explained by intruder sex and by mouse behaviour (Fig. 2h), each imaging frame (sampled at 15 Hz) was manually annotated for one of the following behaviours (on the basis of analysis of synchronous video acquired at 30 Hz): attack, USV^- mount, USV^+ mount, intromission, face-, body- and genital-directed investigation towards male or towards female intruders, approach towards a male or female intruder, and periods of no interaction in the presence of a male or female intruder. We then sampled, for each imaged mouse, an equal number of imaging frames from each of 14 different behavioural conditions (seven male-directed and seven female-directed, selected from the behavioural annotations). The total number of frames sampled varied per imaged mouse, and was set by the behaviour with the fewest imaged frames for that mouse; frames were uniformly sampled in time from the set of frames during which a given behaviour occurred. Having thus defined the set of sampled frames, we constructed for each neuron a $1 \times n$ vector of cell activity $F(t)$ on all frames in the sample set. We regressed the observed activity of all neurons against the sex of the intruder (indicated by a pair of binary vectors) on each of the n frames, and computed the cross-validated error of the fit. We then computed the fraction of variance explained by taking the ratio of the coefficient of determination (R^2) of the fit, divided by the coefficient of determination when $F(t)$ was fit by 14 $1 \times n$ binary vectors representing the presence or absence of each behavioural condition (that is, the maximum explainable variance given the behaviour of the mouse). After subtracting out the signal accounted for by intruder sex, we regressed the residual activity against the identity of the behaviour expressed for each frame, giving variance explained by the female- and male-directed behaviours. The variance 'explained by' intruder sex is simply a correlation, and does not imply that the variance reflects an encoding of intruder sex per se: it may encode sex or some other feature that is tightly correlated with intruder sex (for example, motivation to mount or attack for female versus male intruders, respectively).

Computation of choice probability. The choice probability of each neuron was computed as in previous work[6], which follows its definition in studies of decision-making[43]. In brief, choice probability estimates the accuracy with which two behavioural conditions can be distinguished given the activity of a single neuron. The choice probability of a given neuron for a pair of behavioural conditions is found by constructing a histogram of the activity of that cell ($F(t)$) under each of a selected pair of behavioural conditions, and plotting these histograms against each other to generate a 'receiver operating characteristic' (ROC) curve. The area under this ROC curve is then computed by integration to generate the choice probability value for each unit with respect to each of the two behavioural conditions. This choice probability value is bounded from 0 to 1, with a choice probability of 0.5 indicating that the activity of the neuron cannot distinguish between the two conditions.

The statistical significance of choice probabilities was determined relative to chance, as in previous work[6]. For each neuron, we shuffled behavioural bout timings for the two compared conditions, and computed the choice probability for this shuffled data. Shuffling was repeated 100 times for each of the 2 behaviours, from which we calculated the mean and s.d. (σ) of the 'shuffled' choice probabilities. We considered as significant any observed choice probabilities >2σ above the shuffled mean, and imposed an additional choice probability threshold >0.7. This means that a neuron with a choice probability of, for example, 0.75 can distinguish between the two behaviours of interest with 75% accuracy, and that the probability of correctly predicting which of the two compared behaviours is occurring is significantly greater than when the activity of the neuron is randomized (shuffled) with respect to the actual behavioural annotation for each imaging frame. In Fig. 2k, l, coloured bars indicate the neurons that show a strong and statistically significant choice probability, and grey bars indicate cells for which choice probability was not significantly higher than chance or choice probability ≤ 0.7 for that neuron.

To more confidently distinguish neural representations of behaviour from representations of intruder sex, we computed the choice probability of USV^+ mounting versus female-directed investigation for neurons in MPOA and VMHvl. Because the sex of the intruder during USV^+ mounting and female-directed investigation is the same, we infer that neurons showing a 'preference' (higher $F(t)$) for one behaviour over the other are specifically responding to that behaviour, and not to the sex of the intruder. We then repeated this analysis for the same set of neurons on trials with a male intruder, contrasting USV^- mounting versus male-directed investigation to identify neurons with a preference for USV^- mounting over investigation. The Venn diagrams in Fig. 2m, n then show—for all imaged neurons—what percentage of cells had a statistically significant choice probability (relative to sniff) for USV^+ mounting, USV^- mounting or both behaviours.

Decoding behaviour from neural activity. We trained linear binary SVM decoders to discriminate female-directed USV^+ and male-directed USV^- mounting behaviour from imaged activity of MPOA or VMHvl neurons. Manual annotations of USV^+ and USV^- mounting bouts were used to provide training labels of behaviour type. To decode mounting type as a function of time ('time-evolving decoder') (Fig. 2q, u, Extended Data Fig. 6q, r, u, v), activity $F(t)$ for all imaged cells in a given mouse was divided into 0.4-s bins from 5 s before to 10 s after the onset of mounting. In an effort to remove information about intruder sex from neural activity, for each neuron on each bout we computed the average activity of the cell in a time window from −5 to −3 s of the initiation of mounting, and subtracted this average from $F(t)$ of that cell in all time bins of the bout. For each time bin, we then trained an SVM decoder to discriminate USV^+ from USV^- mounting bouts from the activity of neurons in that bin, using leave-one-out cross-validation across bouts to evaluate decoder accuracy.

Bar graphs of decoder accuracy (Fig. 2r, v Extended Data Fig. 6s, t, w, x) were generated using a 'frame-wise' decoder trained to discriminate USV^+ and USV^- mounting from imaged activity on individual frames of a behaviour (sampled at 15 Hz). Following baseline subtraction (performed as for the time-evolving decoder), USV^+ and USV^- mounting bouts were divided into 'trials', by first merging all bouts of a given behaviour that were separated by less than five seconds (from the end of bout A to the start of bout B). Frames from single- or multi-bout trials were then used to train a linear binary SVM decoder, using leave-one-out cross-validation across intruder mice.

For both decoders, equal numbers of USV^+ and USV^- bouts (time-evolving decoder) or frames (frame-wise decoder) were used during decoder training, to ensure chance decoder performance of 50%. 'Shuffled' decoder data were generated by training the decoder on the same neural data, but with USV^+ and USV^- behaviour annotations randomly assigned to each behaviour bout. Decoding was repeated 20 times for each intruder and each imaged mouse, and decoder performance reported as the average accuracy across imaged mice. For significance testing, the mean accuracy of the decoder trained on shuffled data was computed across mice, and shuffling was repeated 1,000 times. Significance was determined across imaged mice using the Mann–Whitney U test between the mean accuracy of the decoders trained on real versus shuffled data.

Data display. In all the bar graphs, data are expressed as mean ± s.e.m. In all the box-and-whisker plots, centre lines indicate medians, box edges represent the interquartile range and whiskers denote minimal and maximal values.

Statistical analyses. Data were processed and analysed using MATLAB and GraphPad PRISM 8 (GraphPad Software). The sample sizes were chosen on the basis of common practice in animal behaviour experiments. All data were analysed with two-tailed non-parametric tests. In the experiments with paired samples, we used the Wilcoxon matched-pairs signed rank test or Friedman test. In the experiments with non-paired samples, we used the Mann–Whitney U test or Kruskal–Wallis test. All multiple comparisons were corrected with Dunn's multiple comparisons correction. Binary data were analysed with a Fisher's exact test. The significance threshold was held at $\alpha = 0.05$, two-tailed (not significant (NS), $P > 0.05$; *$P < 0.05$; **$P < 0.01$; ***$P < 0.001$; ****$P < 0.0001$). Full statistical analyses corresponding to each dataset are presented in Supplementary Table 2.

Reporting summary

Further information on research design is available in the Nature Research Reporting Summary linked to this paper.

Data availability

The data that support the finding of this study are available from the corresponding author upon request.

Code availability

The custom codes used for pose tracking and behaviour annotation of the mice[5] can be found at GitHub (https://neuroethology.github.io/MARS/). The other code that supports the finding of this study are available from the corresponding author upon request.

30. Vong, L. et al. Leptin action on GABAergic neurons prevents obesity and reduces inhibitory tone to POMC neurons. *Neuron* **71**, 142–154 (2011).
31. Sadowski, P. D. The Flp recombinase of the 2-microns plasmid of *Saccharomyces cerevisiae*. *Prog. Nucleic Acid Res. Mol. Biol.* **51**, 53–91 (1995).
32. Ogawa, S. et al. Abolition of male sexual behaviors in mice lacking estrogen receptors α and β (αβERKO). *Proc. Natl Acad. Sci. USA* **97**, 14737–14741 (2000).
33. Franklin, K. B. J. & Paxinos, G. *The Mouse Brain in Stereotaxic Coordinates* 3rd edn (Academic, 2007).
34. Resendez, S. L. et al. Visualization of cortical, subcortical and deep brain neural circuit dynamics during naturalistic mammalian behavior with head-mounted microscopes and chronically implanted lenses. *Nat. Protoc.* **11**, 566–597 (2016).
35. Zelikowsky, M. et al. The neuropeptide Tac2 controls a distributed brain state induced by chronic social isolation stress. *Cell* **173**, 1265–1279 (2018).
36. Hong, W. et al. Automated measurement of mouse social behaviors using depth sensing, video tracking, and machine learning. *Proc. Natl Acad. Sci. USA* **112**, E5351–E5360 (2015).
37. Kim, C. K. et al. Simultaneous fast measurement of circuit dynamics at multiple sites across the mammalian brain. *Nat. Methods* **13**, 325–328 (2016).
38. Simerly, R. B. & Swanson, L. W. Projections of the medial preoptic nucleus: a *Phaseolus vulgaris* leucoagglutinin anterograde tract-tracing study in the rat. *J. Comp. Neurol.* **270**, 209–242 (1988).
39. Canteras, N. S., Simerly, R. B. & Swanson, L. W. Organization of projections from the ventromedial nucleus of the hypothalamus: a *Phaseolus vulgaris*-leucoagglutinin study in the rat. *J. Comp. Neurol.* **348**, 41–79 (1994).
40. Tachibana, R. O., Kanno, K., Okabe, S., Kobayasi, K. I. & Okanoya, K. USVSEG: a robust method for segmentation of ultrasonic vocalizations in rodents. *PLoS ONE* **15**, e0228907 (2020).
41. Sugimoto, H. et al. A role for strain differences in waveforms of ultrasonic vocalizations during male-female interaction. *PLoS ONE* **6**, e22093 (2011).
42. Zhou, P. et al. Efficient and accurate extraction of in vivo calcium signals from microendoscopic video data. *eLife* **7**, e28728 (2018).

43. Shadlen, M. N. & Newsome, W. T. Neural basis of a perceptual decision in the parietal cortex (area LIP) of the rhesus monkey. *J. Neurophysiol*. **86**, 1916–1936 (2001).
44. Matsumoto, Y. K. & Okanoya, K. Phase-specific vocalizations of male mice at the initial encounter during the courtship sequence. *PLoS ONE* **11**, e0147102 (2016).

Acknowledgements We thank X. Da, J. S. Chang and X. Wang for technical help; Y. Huang for genotyping; Caltech OLAR staff for animal care; J. Costanza for mouse colony management; Inscopix for technical support; C. Segalin and P. Perona for mouse tracking and behaviour classifier software; R. Axel and Y. Oka for constructive comments on the manuscript; C. Chiu for laboratory management; G. Mancuso for administrative assistance; and members of the Anderson laboratory for helpful comments on this project. The illustrations of mice are from TogoTV Picture Gallery (copyright 2016 DBCLS TogoTV). D.J.A. is an investigator of the Howard Hughes Medical Institute. This work was supported by NIH grants R01 MH085082 and R01 MH070053, and a grant from the Simons Collaboration on the Global Brain Foundation (award no. 542947) to D.J.A. T.K. is a recipient of HFSP Long-Term Fellowship. A.K. is a recipient of Helen Hay Whitney Foundation Postdoctoral Fellowship and NIMH K99 Pathway to Independence Award.

Author contributions T.K. and D.J.A conceived and designed the study. T.K. performed and analysed fibre photometry experiments. T.K. and B.Y. performed and analysed micro-endoscope experiments. T.K., M.L. and D.T. performed and analysed optogenetic experiments. T.K. and D.T. performed and analysed chemogenetic experiments and other behaviour experiments. A.K. performed decoder analyses on mouse pose data and micro-endoscope data. I.A.W. wrote the code for the USV detection classifier. T.K. and A.K. prepared figures. T.K. and D.J.A. wrote the paper.

Competing interests The authors declare no competing interests.

Additional information
Supplementary information is available for this paper at https://doi.org/10.1038/s41586-020-2995-0.
Correspondence and requests for materials should be addressed to D.J.A.
Peer review information *Nature* thanks the anonymous reviewers for their contribution to the peer review of this work.
Reprints and permissions information is available at http://www.nature.com/reprints.

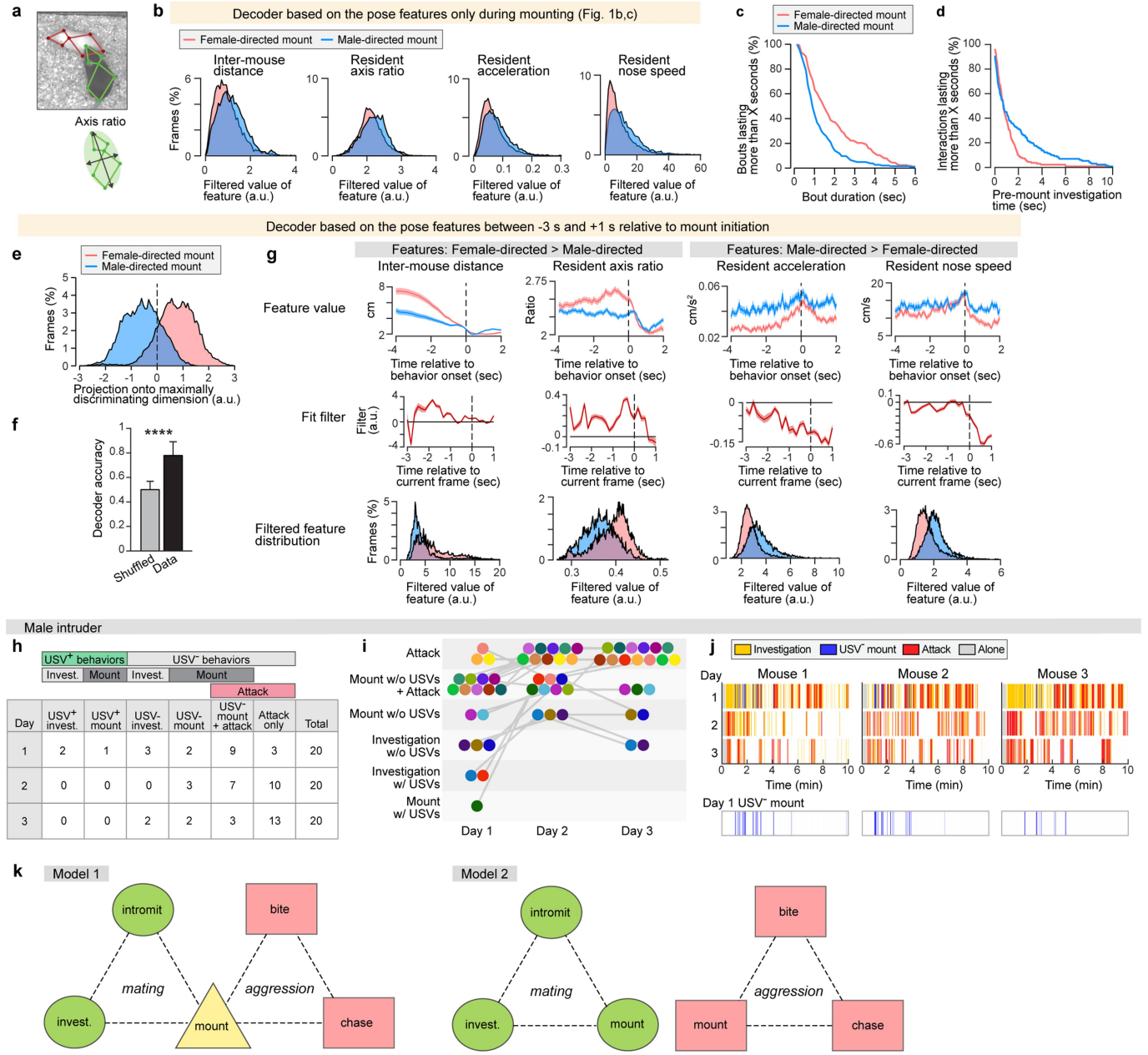

Extended Data Fig. 1 | Additional information for resident–intruder assay with female or male intruders. a, An example of detected resident (green) and intruder (red) key points used for mouse pose estimation (top) and example diagram of the resident 'axis ratio' feature (bottom). **b**, Histograms of values of four relevant mouse pose features during bouts of female- or male-directed mounting. Pose features extracted from mount video frames only are highly overlapping for male- versus female-directed mounts. **c**, Distribution of mounting bout length. **d**, Distribution of time spent in close proximity to the intruder before initiation of mounting. **e**–**g**, Decoding intruder sex from female- versus male-directed mounting from video frames spanning 3 s before to 1 s after mount onset. **e**, Projection of mouse pose features from mounting bouts onto the maximally discriminating dimension of the decoder. **f**, Decoder accuracy compared with shuffled data. Fifty-four behaviour sessions, two-sided Mann–Whitney *U* test, $^{****}P < 0.0001$. **g**, Values of four mouse pose features relative to onset of female- or male-directed mounting (top row), the temporal filter on each feature learned by the SVM decoder (middle row), and histograms of filter output for tested frames of female- versus male-directed interactions, showing separation of feature values (bottom row). a.u., arbitrary units. **h**, **i**, Details of the behaviours of different resident mice towards male intruder across three days, corresponding to Fig. 1g. **h**, Number of mice assigned to each behaviour category. **i**, Visualization of behaviour changes across three days. Different coloured circles indicate different resident mice. Overall, behaviours for each mouse changed from lower intensity categories (less aggressive) to higher intensity categories (more aggressive), with repeated social experience. **j**, Behaviour rasters towards male intruders across three days from three mice. Bottom row indicates extracted USV⁻ mount bouts from day 1 to show that most USV⁻ mounts occur in the early phase of a male–male social interaction. **k**, Two alternative models for encoding of male- versus female-directed mounting in the hypothalamus. In model 1, the two forms of mounting share a common hypothalamic 'mounting control centre'; in model 2, the two forms of mounting use distinct neural substrates. Circles, squares and triangles are abstractions representing different cell populations, and do not correspond to specific nuclei or circuits. Data are mean ± s.e.m. (Supplementary Table 2).

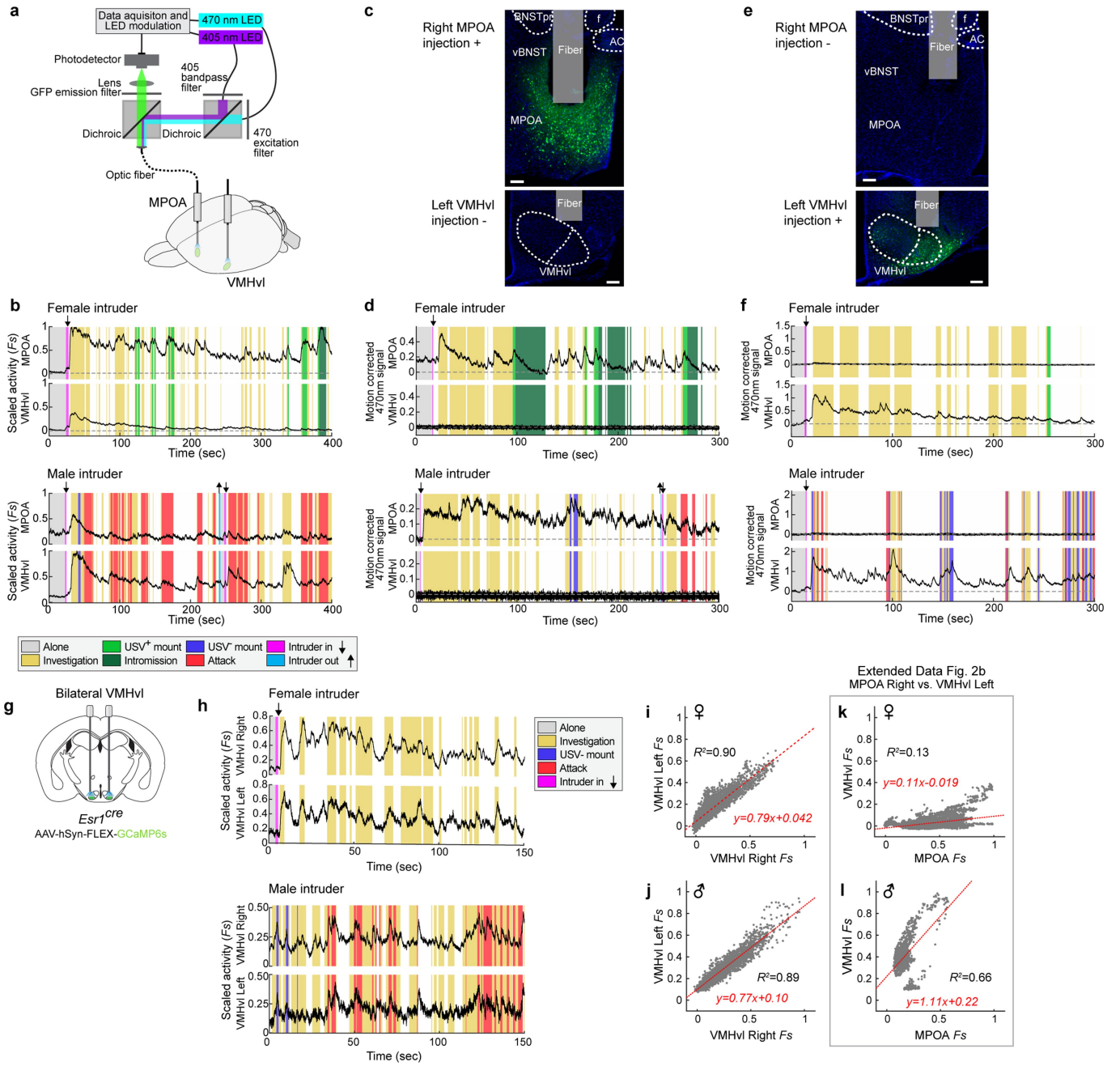

Extended Data Fig. 2 | Control experiment data for dual-site fibre photometry. a, Schematic of dual-site fibre photometry setup. Calcium signals are recorded simultaneously from contralateral MPOA and VMHvl using *Esr1*^{cre} male mice. **b**, Representative scaled calcium signals from MPOA^{ESR1} and VMHvl^{ESR1} neurons after exposure to female (top) and male (bottom) intruders. Vertical shading indicates bouts of annotated social behaviour listed and colour-coded at right. Downward arrows, intruder introduction; upward arrows, intruder removal. **c**–**f**, Representative data from mice injected with GCaMP6s AAV only in MPOA (**c**, **d**), or in VMHvl (**e**, **f**) and recorded from both two areas. **c**, **e**, Representative GCaMP6s expression and optic fibre tract. Top, MPOA; bottom, VMHvl, Scale bars, 100 µm. $n = 2$ each. AC, anterior commissure; f, fornix; BNSTpr, principal division of the bed nucleus of the stria terminalis; vBNST, ventral BNST; fiber, optic fibre tract. **d**, **f**, Representative GCaMP6s traces from MPOA^{ESR1} and VMHvl^{ESR1} neurons with female and male intruders. Vertical shading indicates bouts of annotated social behaviour listed and colour-coded at right. Data are presented as raw motion corrected 470-nm traces. Non-injected sites (VMHvl in **c**, MPOA in **e**) had few GCaMP-positive fibres from contralateral injection sites (**c**, **e**) and did not show detectable Ca^{2+} signal changes (flat lines in **d**, **f**). **g**–**j**, Representative data from recording bilateral VMHvl^{ESR1} neurons. $n = 2$. **g**, Schematic of fibre photometry recording from bilateral VMHvl. **h**, Ca^{2+} traces from female and male trials. Ca^{2+} traces in right and left hemispheres are highly correlated. **i**, **j**, Distribution of scaled activity in right (x axis) versus left (y axis) VMHvl^{ESR1} neurons across entire trials with female (**i**) and male (**j**) intruders. Activity was fitted to $y = ax + b$ (red line) using 1-kHz sampling traces and scatter plots display downsampled (30 Hz) time points. R^2, coefficient of determination. **k**, **l**, Distribution of scaled activity in MPOA^{ESR1} (x axis) versus VMHvl^{ESR1} (y axis) neurons across entire trials with female (**k**) and male (**l**) intruders from the traces in **b**. MPOA^{ESR1} and VMHvl^{ESR1} neural activities are less correlated than bilateral VMHvl^{ESR1} neural activities.

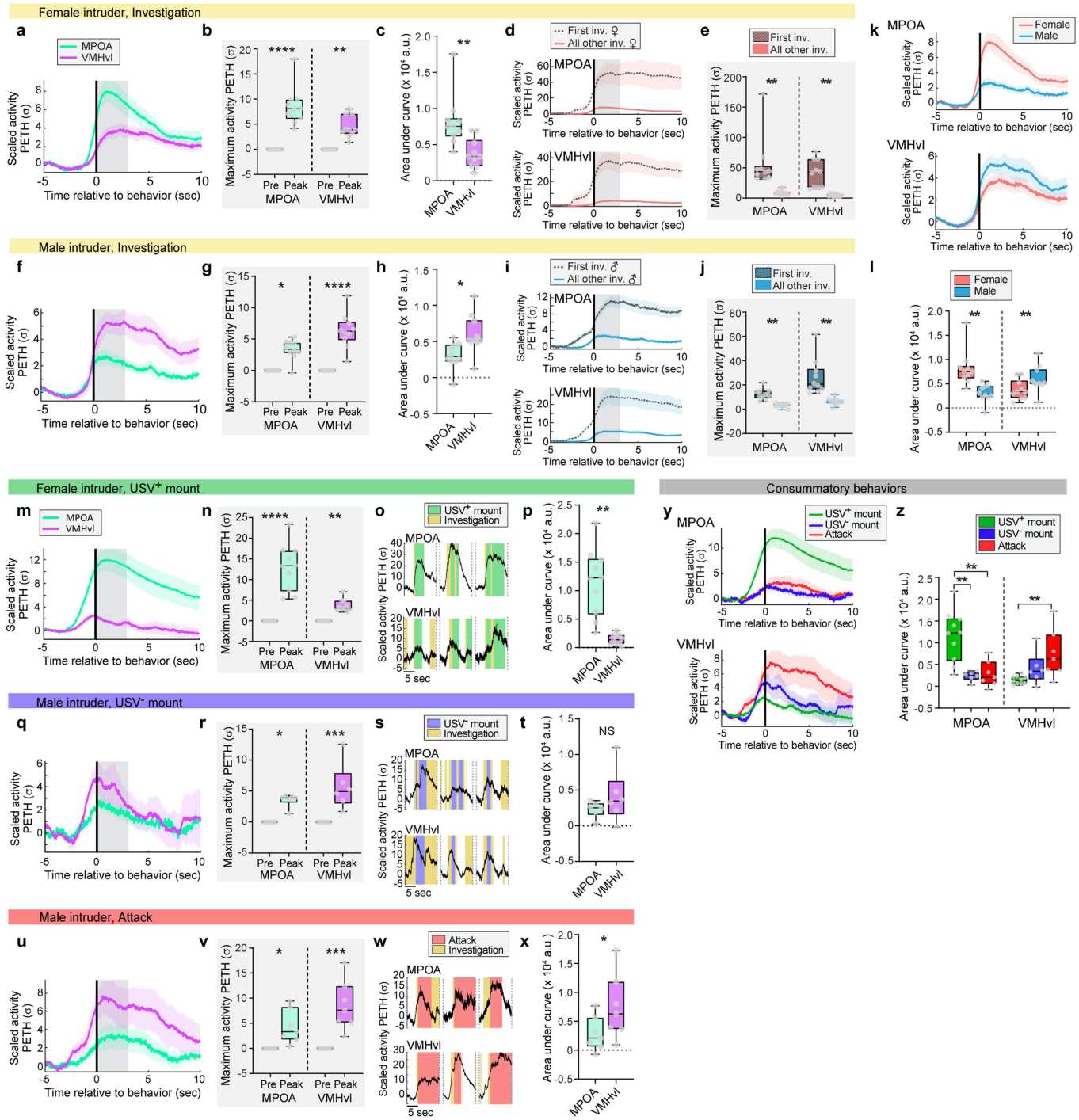

Extended Data Fig. 3 | See next page for caption.

Extended Data Fig. 3 | Dual-site fibre photometry recording during social interaction. a–**j**, Average calcium signals in MPOA^{ESR1} and in VMHvl^{ESR1} neurons aligned to social investigation onset of female (**a**–**e**) and male (**f**–**j**) intruders. $n = 10$. First investigation bouts of each intruder have stronger calcium signals than all other investigation bouts and were analysed separately (**d**, **e**, **i**, **j**). **a**, **f**, PETH of scaled neural activity normalized to pre-behaviour period. **b**, **g**, Maximum PETH signal during 0 to 3 s from investigation onset (shaded grey area in **a**, **f**), compared with mean activity during pre-behaviour period (−5 to −3 s). **b**, $^{****}P < 0.0001$, $^{**}P = 0.0025$; **g**, $^{*}P = 0.0105$, $^{****}P < 0.0001$. **c**, **h**, Integrated activity during investigation. **c**, $^{**}P = 0.0039$; **h**, $^{*}P = 0.0273$. a.u., arbitrary units. **d**, **e**, **i**, **j**, Average calcium signals during first investigation of each intruder versus all other investigation bouts towards female (**d**, **e**) and male (**i**, **j**) intruders. **d**, **i**, PETH of scaled neural activity. **e**, **j**, Maximum PETH signal during 0 to 3 s from first investigation onset. **e**, **j**, $^{**}P = 0.002$. **k**, **l**, Average calcium signals during social investigation in each region. **k**, PETH of scaled neural activity in MPOA^{ESR1} and VMHvl^{ESR1}. $n = 10$. Traces were reproduced and rescaled from data in **a**, **f** for comparative purposes. **l**, Integrated activity during investigation. $^{**}P = 0.0098$ (MPOA), 0.0059 (VMHvl). **m**–**x**, Average calcium signals during USV^{+} mounts towards female intruders (**m**–**p**, $n = 10$), USV^{-} mounts towards male intruders (**q**–**t**, $n = 6$) or attack towards male intruders (**u**–**x**, $n = 7$). **m**, **q**, **u**, PETH of average scaled neural activity. **n**, **r**, **v**, Maximum scaled activity during 0–3 s from behaviour onset. **n**, $^{****}P < 0.0001$, $^{**}P = 0.0014$; **r**, $^{*}P = 0.0358$, $^{***}P = 0.0009$; **v**, $^{*}P = 0.0104$, $^{***}P = 0.0007$. **o**, **s**, **w**, Representative PETH traces for each behaviour. Coloured shading marks behavioural episodes. **p**, **t**, **x**, Integrated activity in during behaviours. **p**, $^{**}P = 0.002$; **x**, $^{**}P = 0.0469$. **m** and **q** traces were reproduced and rescaled from data in Fig. 2c. **y**, Average calcium signals during USV^{+} mount, USV^{-} mount and attack. **y**, PETH of scaled activity in MPOA^{ESR1} and VMHvl^{ESR1}neurons. USV^{+} mount, $n = 10$; USV^{-} mount, $n = 6$; attack, $n = 7$. Traces were reproduced and rescaled from data in **m**, **q** and **u**. **z**, Integrated activity during each behaviour. $^{**}P = 0.0092$, 0.0097, 0.0097 (left to right). **b**, **e**, **g**, **j**, **l**, **n**, **r**, **v**, **z**, Kruskal–Wallis test; **c**, **h**, **p**, **t**, **x**, Wilcoxon test. Data are mean ± s.e.m. except for box plots (see Fig. 2 legend). All statistical tests are two-sided and corrected for multiple comparisons when necessary (Supplementary Table 2).

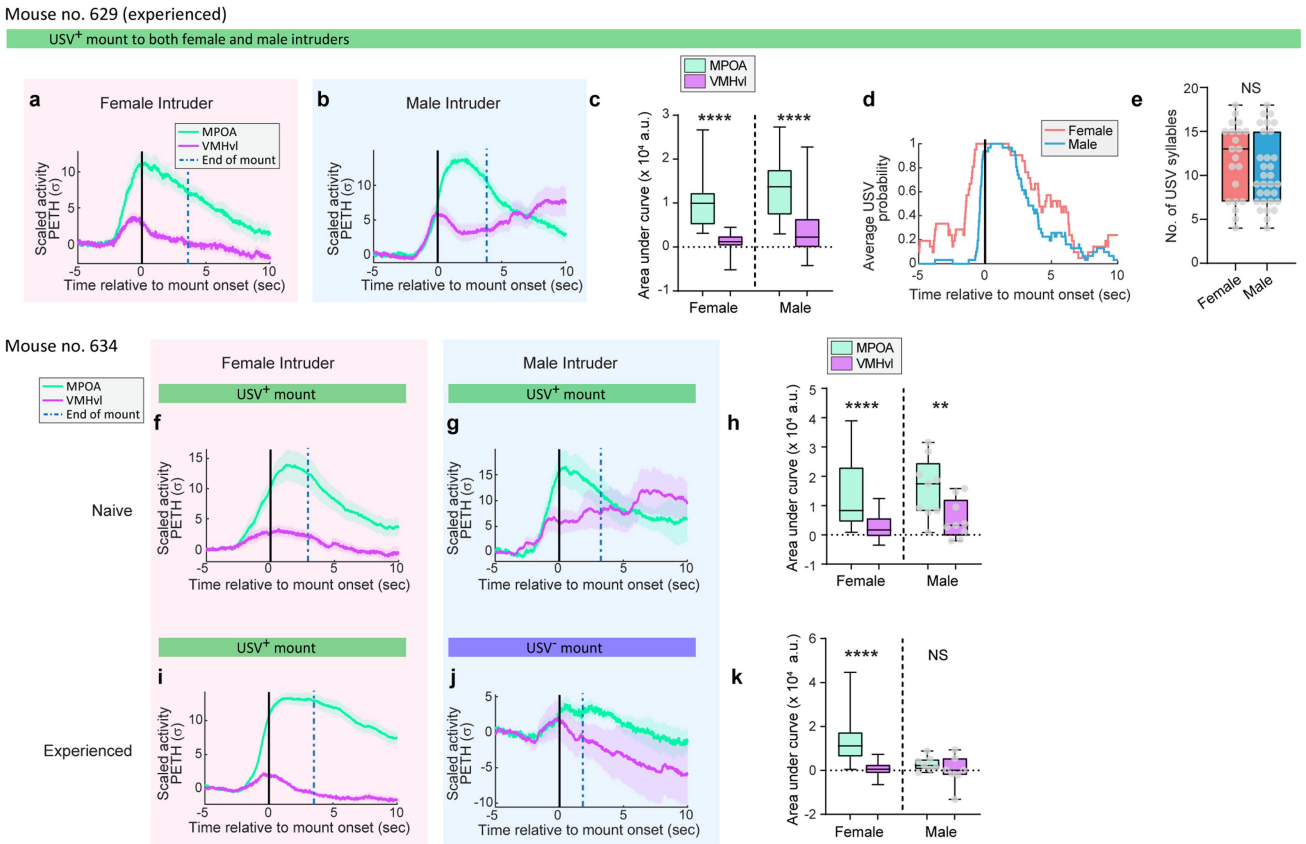

Extended Data Fig. 4 | Neural activity patterns in rare mice that exhibit USV⁺ mounting towards male intruders resemble those observed during USV⁺ mount towards female intruders. a–**e**, Calcium activity and USV data from a sexually and socially experienced mouse (no. 629) that showed USV⁺ mounting towards both female and male intruders. Female, 21 bouts; male, 30 bouts. **a**, **b**, PETH traces aligned at onset of USV⁺ mount towards female (**a**) or male (**b**) intruders. **c**, Integrated activity during mounting bouts. $^{****}P < 0.0001$. **d**, **e**, Quantification of USVs from mouse no. 629 towards female or male intruders. **d**, Distribution of USVs aligned at onset of USV⁺ mount. **e**, Number of USV syllables during 0 to 5 s from onset of USV⁺ mount. This mouse did not display any attack behaviour towards male mice, but preferred females to males in a triadic interaction test (Supplementary Note 2). **f**–**k**, Calcium activity data from one mouse (no. 634) which showed USV⁺ mounting towards males when sexually and socially naive, and later USV⁻ mounting after it obtained sexual and social experience. **f**, **g**, PETH traces from naive mouse aligned at onset of USV⁺ mount. **h**, Integrated activity during mounting bouts from data in **f**, **g**. Female, 27 bouts; male, 9 bouts, $^{****}P < 0.0001$, $^{**}P = 0.0039$. **i**, **j**, PETH traces from the same mouse after social and sexual experience, aligned at onset of USV⁺ mounting towards female or USV⁻ mounting towards male intruders. **k**, Integrated activity during mounting bouts from traces in **i**, **j**. Female, 107 bouts; male, 7 bouts, $^{****}P < 0.0001$. **c**, **h**, **k**, Wilcoxon test; **e**, Mann–Whitney *U* test. Data are mean ± s.e.m. except for box plots (see Fig. 2 legend). All statistical tests are two-sided and corrected for multiple comparisons when necessary (Supplementary Table 2).

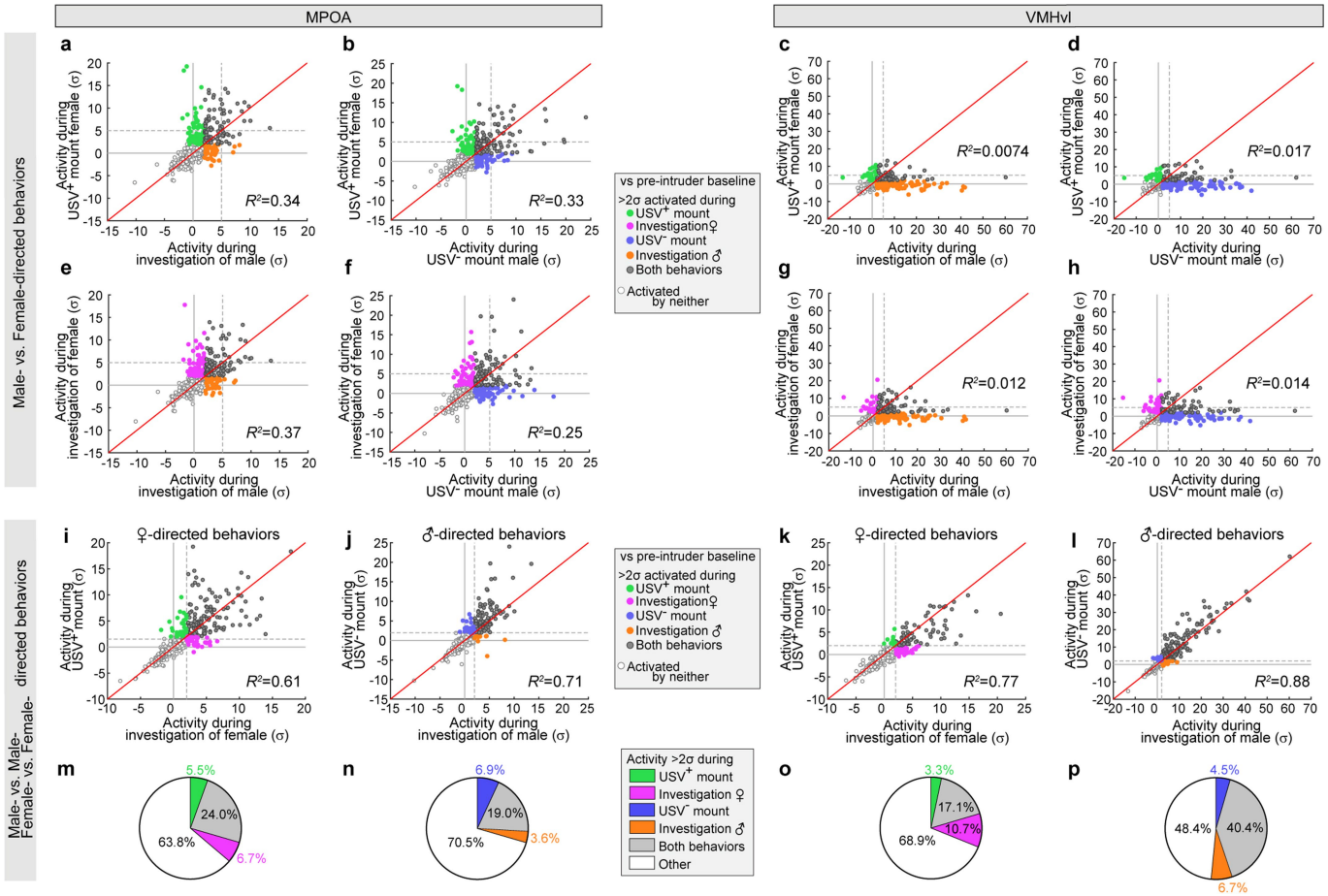

Extended Data Fig. 5 | Correlation of ESR1⁺ neural activity during male- versus female-, male- versus male-, or female- versus female-directed behaviours in MPOA and VMHvl. a–**l**, Average calcium response per neuron in MPOA^{ESR1} (**a**, **b**, **e**, **f**, **i**, **j**) or VMHvl^{ESR1} (**c**, **d**, **g**, **h**, **k**, **l**) populations during female-directed behaviours (USV⁺ mounting or investigation, *y* axis) versus male-directed behaviours (USV⁻ mounting or investigation, *x* axis) (**a**–**h**), female-directed USV⁺ mounting (*y* axis) versus investigation (*x* axis) (**i**, **k**) or male-directed USV⁻ mounting (*y* axis) versus investigation (*x*-axis) (**j**, **k**), compared to pre-intruder baseline period. Coloured points indicate cells with >2*σ*, compared to pre-intruder baseline period. Red lines, $y = x$. R^2, coefficient of determination. Dashed lines, 2*σ*. **m**–**p**, Proportion of cells excited (>2*σ*) during female- (**m**, **o**) or male- (**n**, **p**) directed behaviours. The correlations of the neural activity during the behaviours directed towards the same sex (**i**–**l**) are higher than the correlations during the behaviours directed towards the different sex (**a**–**h**).

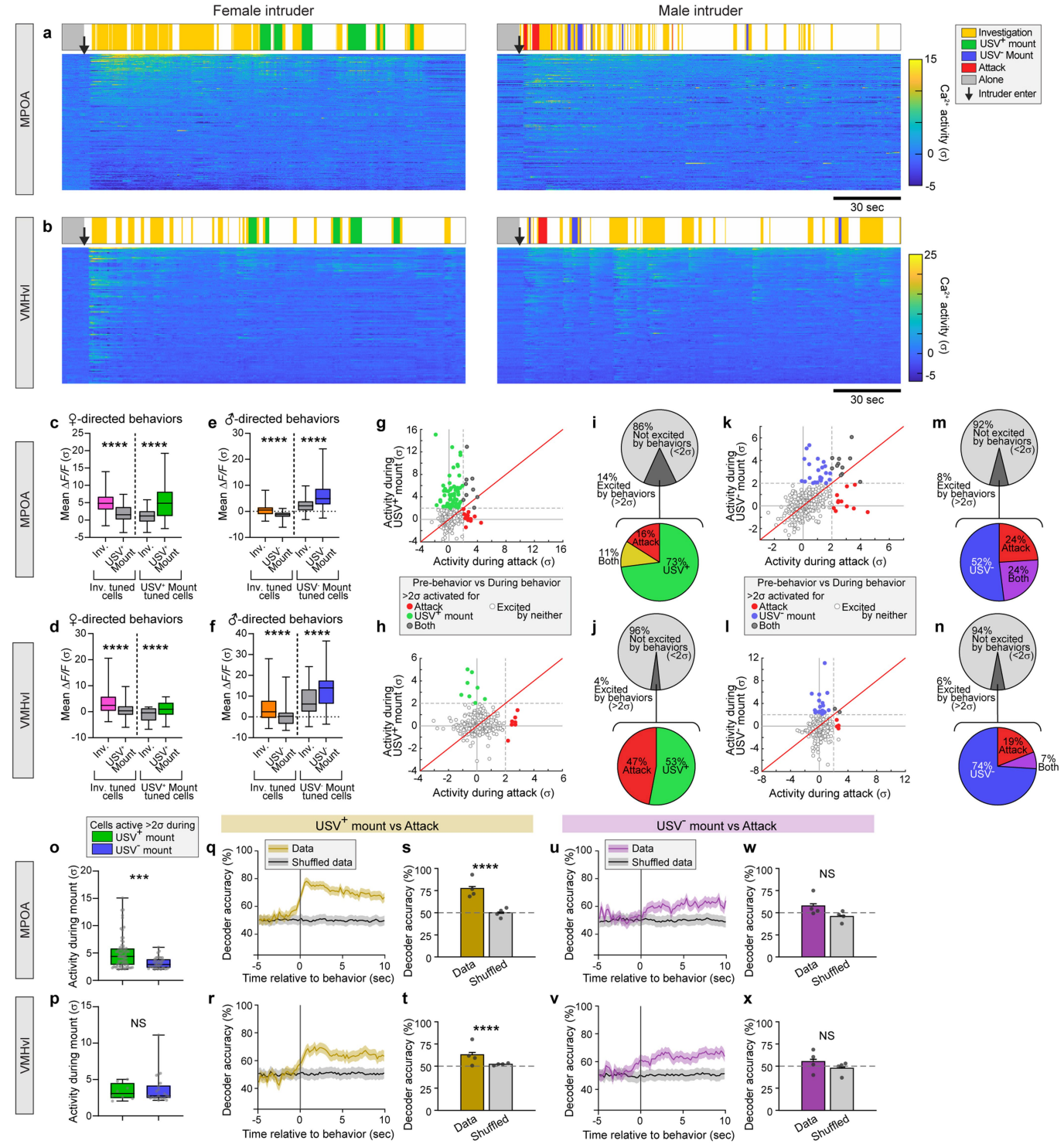

Extended Data Fig. 6 | See next page for caption.

Extended Data Fig. 6 | Neuronal population representations of social behaviours in MPOA and VMHvl. a, **b**, Representative calcium activity rasters of $MPOA^{ESR1}$ (**a**) and $VMHvl^{ESR1}$ (**b**) neurons during social interaction with a female (left) or male (right) intruder, sorted by mean activity level during the displayed period. Behaviours of the resident mice are indicated above the neural activity rasters. Arrows, intruder introduction. **c**–**f**, Response strength of behaviour-tuned populations, during their preferred behaviour (coloured bars) and non-preferred behaviour (grey bars). Behaviour-tuned populations are defined by choice probability for female-directed mount versus investigation (**c**, **d**, from Fig. 2k, l, left) and for male-directed mount versus investigation (**e**, **f**, from Fig. 2k, l, right). **c**, $n = 41$ (inv-tuned), 53 (mount-tuned); **d**, $n = 61$ (inv), 12 (mount); **e**, $n = 38$ (inv), 63 (mount); **f**, $n = 21$ (inv), 24 (mount), $^{****}P < 0.0001$, $^{***}P = 0.0005$. **g**–**n**, Average calcium response per neuron during female-directed USV^+ mounting (*y* axis) versus male attack (*x* axis) (**g**–**j**), and male-directed USV^- mounting (*y* axis) versus male attack (*x* axis) (**k**–**n**), relative to activity immediately before behaviour initiation. **g**, **h**, **k**, **l**, Scatter plots. **i**, **j**, **m**, **n**, Proportion of cells excited (>2σ) during each behaviour. **o**, **p**, Average response strength of mount responsive neurons (>2σ relative to activity immediately before mount initiation). USV^+ mount-responsive neurons (green + grey dots in Fig. 2o, s), $n = 68$ (MPOA), 8 (VMHvl); USV^- mount-responsive (blue + grey dots in Fig. 2o, s), $n = 35$ (MPOA), 22 (VMHvl), $^{***}P = 0.0001$. **q**–**x**, Accuracy of time-evolving (**q**, **r**, **u**, **v**) or frame-wise (**s**, **t**, **w**, **x**) decoders predicting USV^+ mounting from attack (**q**–**t**) and USV^- mounting from attack (**u**–**x**), trained on neural activity. $n = 4$, $^{****}P < 0.0001$, $^{*}P = 0.026$. **c**–**f**, Wilcoxon test; **o**, **p**, **s**, **t**, **w**, **x**, Mann–Whitney *U* test. Data are mean ± s.e.m. except for box plots (see Fig. 2 legend). All statistical tests are two-sided and corrected for multiple comparisons when necessary (Supplementary Table 2).

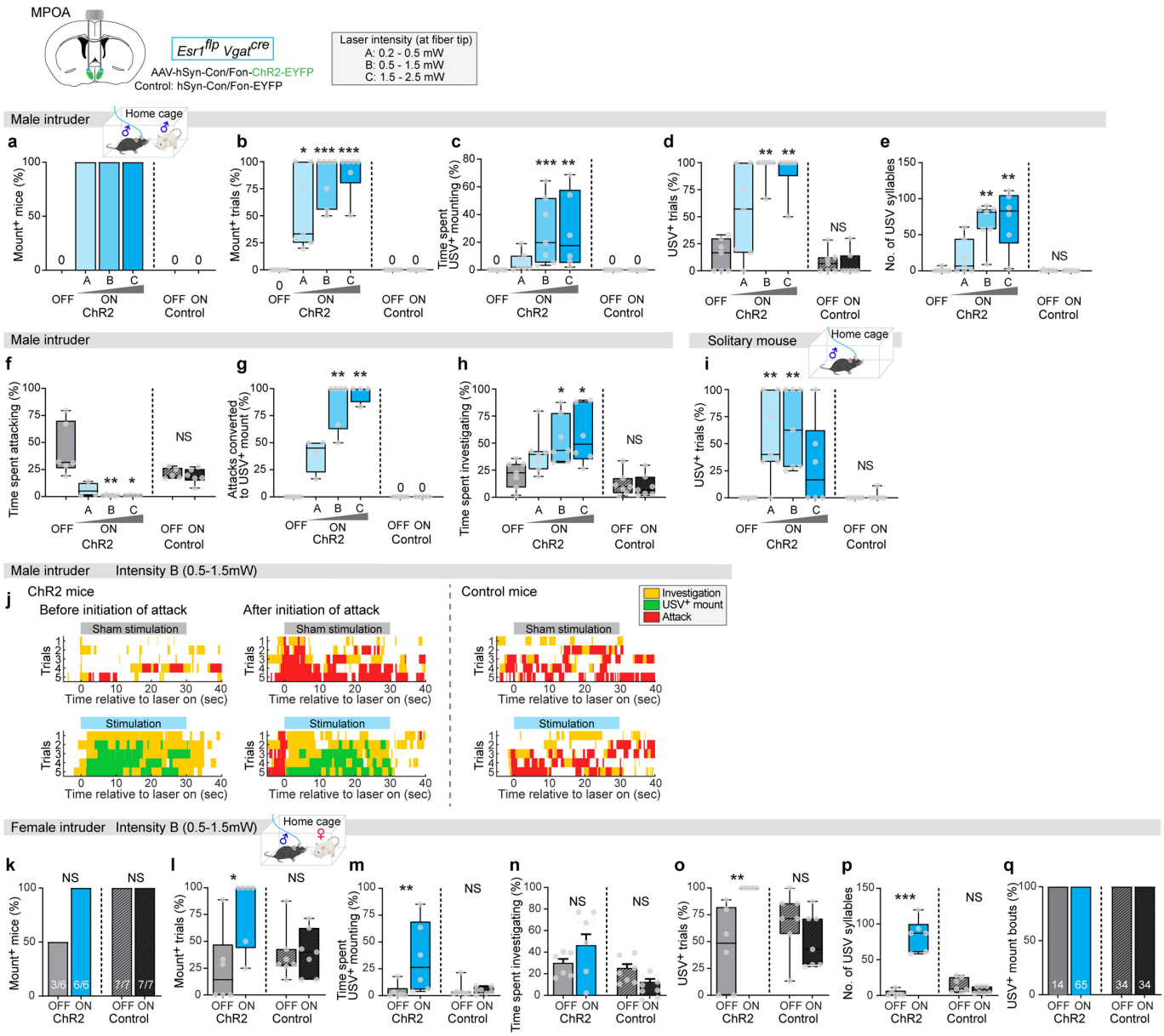

Extended Data Fig. 7 | Stimulation of MPOA$^{ESR1\cap VGAT}$ neurons triggers mounting and USVs towards male and female intruders. **a**–**i**, Quantification of behaviour parameters towards male intruders (**a**–**h**) or under solitary conditions (**i**) with different laser intensities. **a**–**f**, **h**, **i**, ChR2 with intensity A, B, off, $n = 7$; C, $n = 6$; control, $n = 7$; **g**, ChR2 with intensity B and off, $n = 6$; A and C, $n = 6$; control, on $n = 5$, off $n = 4$. Data with intensity B (0.5–1.5 mW) are reproduced from Fig. 3 for comparative purposes. **b**, Left to right, $^{*}P = 0.0418$, $^{***}P = 0.0009, 0.0006$. **c**, $^{***}P = 0.0004$, $^{**}P = 0.001$. **d**, $^{**}P = 0.0012, 0.0031$. **e**, $^{**}P = 0.0025, 0.0024$. **f**, $^{**}P = 0.0027$, $^{**}P = 0.0179$. **g**, $^{**}P = 0.0014, 0.002$. **h**, $^{*}P = 0.0102, 0.0112$. **i**, $^{**}P = 0.0096, 0.0045$. **j**, Representative behaviour raster plots towards male intruders from ChR2 and control mice without (top) and with (bottom) photostimulation with laser intensity B (0.5–1.5 mW). **k**–**q**, Quantification of behaviour parameters towards female intruders with laser intensity B (0.5–1.5 mW). ChR2, $n = 6$; control, $n = 7$. **l**, $^{*}P = 0.0127$. **m**, $^{**}P = 0.0034$. **o**, $^{**}P = 0.0025$. **p**, $^{***}P = 0.0001$. **b**–**i** (ChR2), **l**–**p**, Kruskal–Wallis test; **b**–**i** (control), Wilcoxon test; **k**, Fisher's test. Data are mean ± s.e.m. except for box plots (see Fig. 2 legend). All statistical tests are two-sided and corrected for multiple comparisons when necessary (Supplementary Table 2).

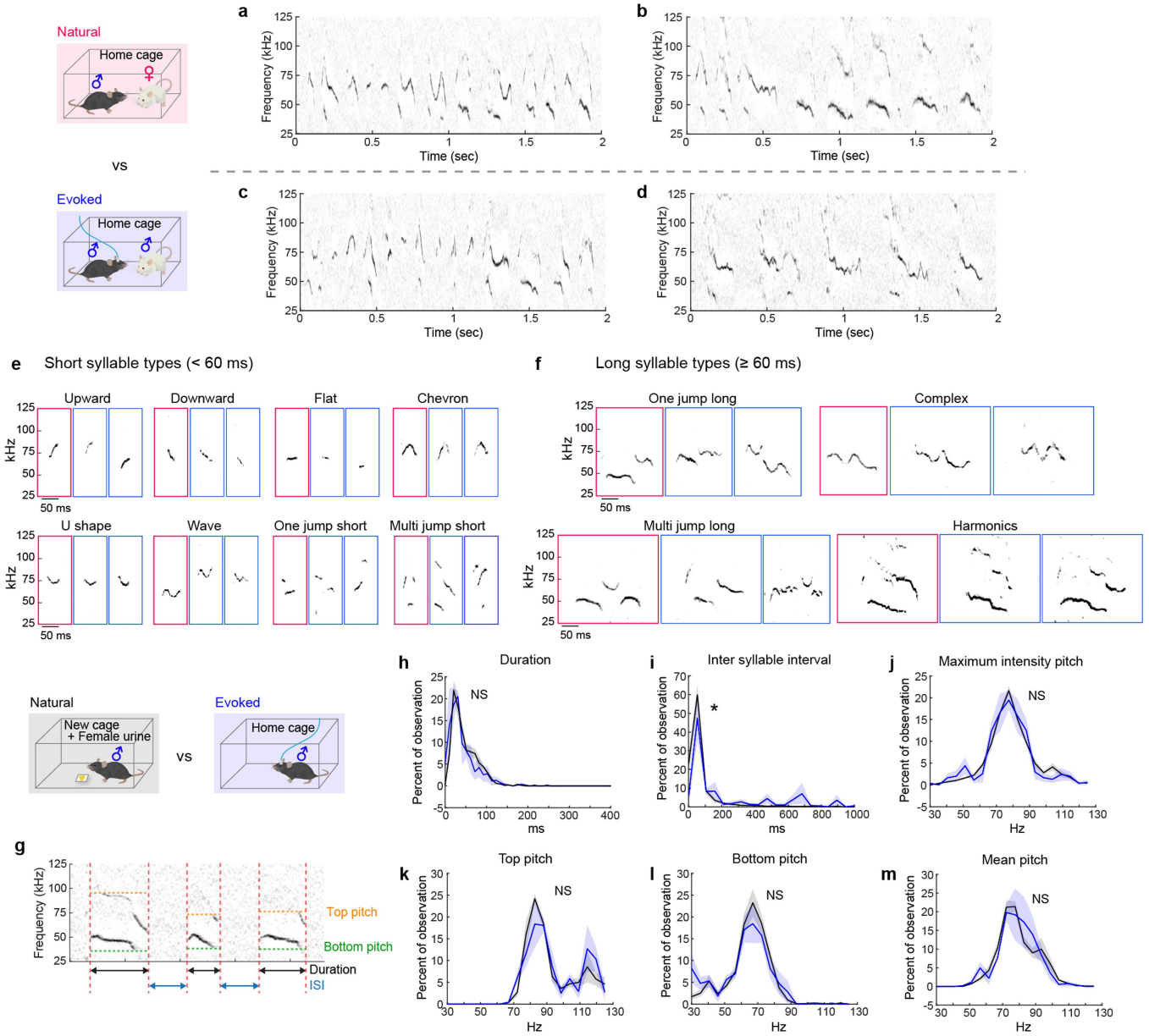

Extended Data Fig. 8 | Comparison between features of naturally occurring and optogenetically evoked USVs. a–d, Example spectrograms from male–female interaction (natural USVs, **a**, **b**) and male–male interaction during MPOA$^{ESR1\cap VGAT}$ optogenetic stimulation (evoked USVs, **c**, **d**). **e**, **f**, Example syllables extracted from naturally occurring USVs recorded during male–female interactions (pink), and from evoked USVs recorded during male–male interactions with MPOA optogenetic stimulation (blue). Syllable were first classified into short (duration <60 ms, **e**) or long (≥60 ms, **f**), then further manually classified into total of 12 categories according to previous criteria[44]. All 12 syllable types were observed among both natural and evoked USVs. **g–m**, Comparison of acoustic features between USVs evoked by female urine or optogenetic stimulation of MPOA in solitary males. **g**, Schematic of the acoustic parameters of USVs (Methods). ISI, inter syllable interval. **h–m**, Histograms of acoustic features. Optogenetically evoked USVs in solitary males (blue, 3 mice), natural USVs evoked by female urine (black, 5 mice). Asterisk indicates significant difference between the distributions of the feature from natural versus evoked USVs. Kolmogorov–Smirnov test, **i**, $^*P < 0.0001$. Number of syllables used in the analysis, ISI, natural $n = 844$, evoked $n = 263$; other features, natural $n = 868$, evoked $n = 285$. Data are mean ± s.e.m. (Supplementary Table 2).

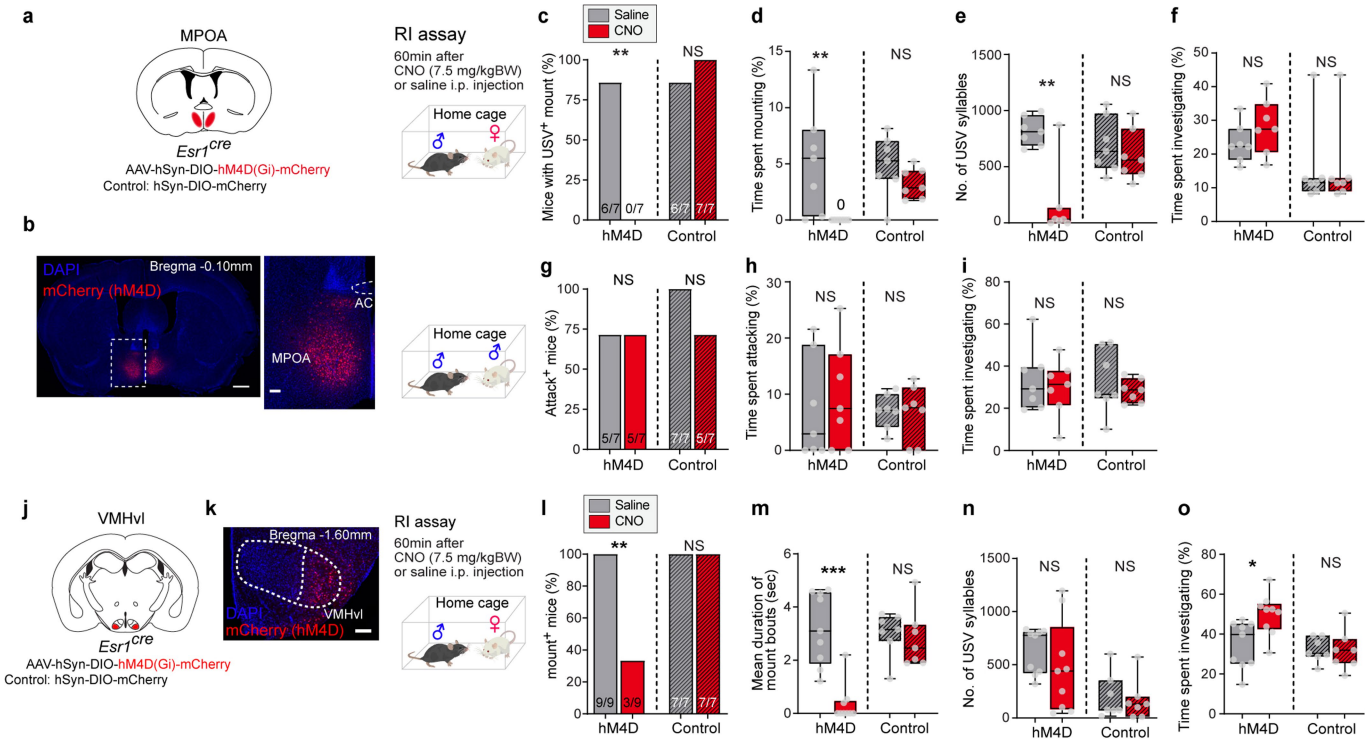

Extended Data Fig. 9 | Chemogenetic inhibition of MPOA^{ESR1} and VMHvl^{ESR1} neurons decreases mounting towards females. a, Strategy to chemogenetically inhibit MPOA^{ESR1} neurons in male *Esr1^{cre}* mice. **b**, mCherry (hM4D) expression in MPOA in *Esr1^{cre}* mice with boxed region magnified (right). Scale bars, 500 µm (left), 100 µm (right). $n = 7$. **c**–**f**, Behaviour parameters from resident–intruder (RI) assay with female intruders. hM4D, $n = 7$; control, $n = 7$. **c**, Per cent mice showing USV^{+} mounting, $^{**}P = 0.0047$. **d**, Per cent time spent USV^{+} mounting, $^{**}P = 0.0034$. **e**, Number of USV syllables, $^{**}P = 0.0021$. **f**, Per cent time spent investigating. **g**–**i**, Behaviour parameters from resident–intruder assay with male intruders. **g**, Per cent mice showing attack. **h**, Per cent time spent attacking, **i**, Per cent time spent investigating. **j**, Strategy to chemogenetically inhibit VMHvl^{ESR1} neurons in male *Esr1^{cre}* mice. **k**, mCherry (hM4D) expression in VMHvl. Scale bar, 100 µm. $n = 9$. **l**–**o**, Behaviour parameters from resident–intruder assay with female intruders. hM4, $n = 9$; control, $n = 7$. **l**, Per cent mice showing USV^{+} mounting, $^{**}P = 0.009$. **m**, Mean duration of USV^{+} mount bouts, $^{***}P = 0.0008$. **n**, Number of USV syllables. **o**, Per cent time spent investigating, $^{*}P = 0.024$. **c**, **g**, **l**, Fisher's test; **d**–**f**, **h**, **i**, **m**–**o**, Kruskal–Wallis test. In box plots, centre lines indicate medians, box edges represent the interquartile range and whiskers denote minimal and maximal values. All statistical tests are two-sided and corrected for multiple comparisons when necessary (Supplementary Table 2).

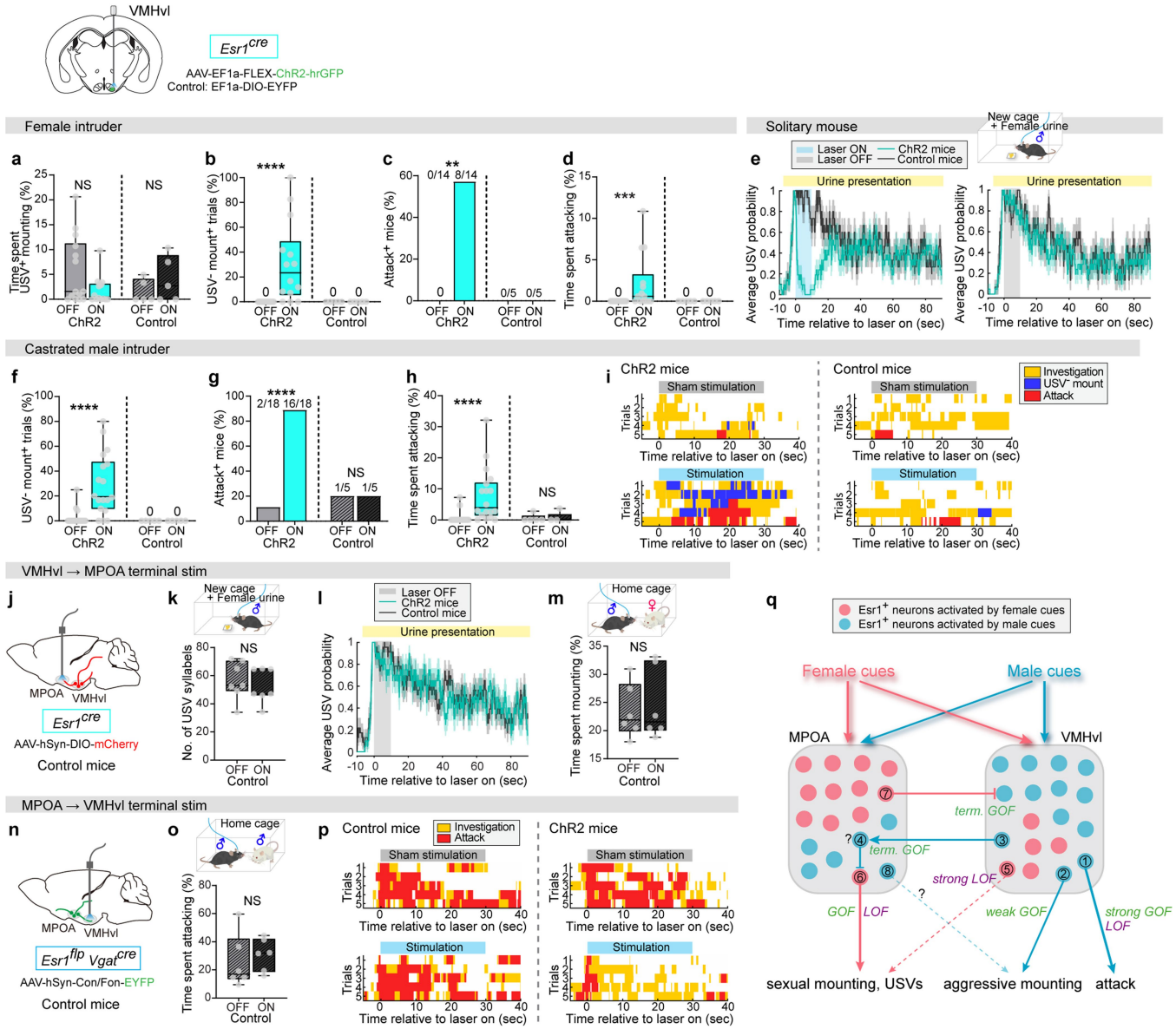

Extended Data Fig. 10 | Optogenetic stimulation of VMHvl^{ESR1} neurons triggers USV$^-$ mounting as well as attack towards female and castrated male intruders. **a**–**i**, Behaviours during photostimulation towards female intruders (**a**–**d**), alone with female urine presentation (**e**) or towards castrated male intruders (**f**–**i**). **a**, Per cent time spent USV$^+$ mounting. **b**, **f**, Fraction of trials with USV$^-$ mounting, $^{****}P < 0.0001$. **c**, **g**, Fraction of mice showing attack, $^{**}P = 0.0019$, $^{****}P < 0.0001$. **d**, **h**, Per cent time spent attacking, $^{****}P < 0.0001$. **e**, Probability of USVs with (left) and without photostimulation (right). ChR2, $n = 7$; control, $n = 5$, **i**, Behaviour raster plots from ChR2 (left) and control mice (right). **a**–**d**, $n = 14$ (ChR2), 5 (control). **e**, $n = 7$ (ChR2), 7 (control). **f**–**h**, $n = 18$ (ChR2), 5 (control). **j**–**m**, Controls for optogenetic activation of ESR1$^{VMHvl \rightarrow MPOA}$ axon terminals. **j**, Schematic. **k**, Number of USV syllables evoked by female urine during photostimulation with control mice. **l**, Probability of USVs with sham photostimulation. $n = 7$ (ChR2, cyan), 7 (control, grey). **m**, Per cent time spent USV$^+$ mounting during photostimulation with control mice, triggered after mount onset. $n = 6$. **n**–**p**, Controls for optogenetic activation of ESR1∩VGAT$^{MPOA \rightarrow VMHvl}$ axon terminals. **n**, Schematic. **o**, Per cent time spent attacking during photostimulation with control mice. $n = 6$. **p**, Behaviour raster plots with male intruders from control (left) and ChR2 mice (right). **q**, Working hypothesis to reconcile imaging experiments and effects of functional manipulations of ESR1$^+$ neurons in MPOA and VMHvl. Small circles are ESR1$^+$ neurons, pink circles are neurons preferentially activated by female cues and blue circles are neurons preferentially activated by male cues. GOF, gain-of-function manipulation of neuronal activity (optogenetic or chemogenetic activation); LOF, loss-of-function manipulation of neuronal activity (optogenetic or chemogenetic). term. GOF, optogenetic stimulation of nerve terminals. See Supplementary Note 3 for details and explanations about the numbers in the neurons. **a**, **b**, **d**, **f**, **h**, **k**, **m**, **o**, Kruskal–Wallis test; **c**, **g**, Fisher's test. Data are mean ± s.e.m. except for box plots (see Fig. 2 legend). All statistical tests are two-sided and corrected for multiple comparisons when necessary (Supplementary Table 2).

nature research

Corresponding author(s): David J. Anderson

Last updated by author(s): 8/31/2020

Reporting Summary

Nature Research wishes to improve the reproducibility of the work that we publish. This form provides structure for consistency and transparency in reporting. For further information on Nature Research policies, see Authors & Referees and the Editorial Policy Checklist.

Statistics

For all statistical analyses, confirm that the following items are present in the figure legend, table legend, main text, or Methods section.

n/a	Confirmed
☐	☒ The exact sample size (*n*) for each experimental group/condition, given as a discrete number and unit of measurement
☐	☒ A statement on whether measurements were taken from distinct samples or whether the same sample was measured repeatedly
☐	☒ The statistical test(s) used AND whether they are one- or two-sided *Only common tests should be described solely by name; describe more complex techniques in the Methods section.*
☐	☒ A description of all covariates tested
☐	☒ A description of any assumptions or corrections, such as tests of normality and adjustment for multiple comparisons
☐	☒ A full description of the statistical parameters including central tendency (e.g. means) or other basic estimates (e.g. regression coefficient) AND variation (e.g. standard deviation) or associated estimates of uncertainty (e.g. confidence intervals)
☐	☒ For null hypothesis testing, the test statistic (e.g. *F*, *t*, *r*) with confidence intervals, effect sizes, degrees of freedom and *P* value noted *Give P values as exact values whenever suitable.*
☒	☐ For Bayesian analysis, information on the choice of priors and Markov chain Monte Carlo settings
☒	☐ For hierarchical and complex designs, identification of the appropriate level for tests and full reporting of outcomes
☒	☐ Estimates of effect sizes (e.g. Cohen's *d*, Pearson's *r*), indicating how they were calculated

Our web collection on statistics for biologists contains articles on many of the points above.

Software and code

Policy information about availability of computer code

Data collection	StreamPix 7 for behavior video acquisition, Avisoft-RECORDER USGH for Audio recording, Inscopix data acquisition software for microendoscope recording, Synapse for fiber photometry recording
Data analysis	Python2.7 for Animal pose tracking with custom codes (https://neuroethology.github.io/MARS/), MATLAB 2018b for analyzing behaviors and calcium imaging data, GraphPad Prism 8 and MATLAB 2018b for statistical analyses, Adobe Illustrator Ver.24 for assembling figures, Adobe Premiere Pro Ver.14 for video rendering

For manuscripts utilizing custom algorithms or software that are central to the research but not yet described in published literature, software must be made available to editors/reviewers. We strongly encourage code deposition in a community repository (e.g. GitHub). See the Nature Research guidelines for submitting code & software for further information.

Data

Policy information about availability of data

All manuscripts must include a data availability statement. This statement should provide the following information, where applicable:

- Accession codes, unique identifiers, or web links for publicly available datasets
- A list of figures that have associated raw data
- A description of any restrictions on data availability

The data that support the finding of this study are available from the corresponding author upon request.

Field-specific reporting

Please select the one below that is the best fit for your research. If you are not sure, read the appropriate sections before making your selection.

☒ Life sciences ☐ Behavioural & social sciences ☐ Ecological, evolutionary & environmental sciences

For a reference copy of the document with all sections, see nature.com/documents/nr-reporting-summary-flat.pdf

Life sciences study design

All studies must disclose on these points even when the disclosure is negative.

Sample size	No statistics were used to determine sample sizes. Sample sizes were determined based on our previous experiments to sufficiently detect meaningful biological differences with good reproducibility (Lee et al., 2014, and Remedios and Kennedy et al., 2017, cited in the manuscript).
Data exclusions	Animals in which the virus injection and/or implantation missed the target brain region were excluded from analysis.
Replication	All the experiments were repeated at least two times with separate cohort of animals, and the reproducibility was confirmed.
Randomization	For functional manipulation experiments, about half of the mice in each cage were randomly assigned to either control or experimental groups. All control mice were treated with the same experimental procedures, except a control virus was injected instead. For imaging experiments, animals were randomly chosen from Esr1-Cre transgenic cohort. The order of male or female intruder experiments were performed in the random order in imaging experiments, but were not randomized in functional manipulation experiments.
Blinding	The experimenter was blind to experimental or control groups during data collection and analyses.

Reporting for specific materials, systems and methods

We require information from authors about some types of materials, experimental systems and methods used in many studies. Here, indicate whether each material, system or method listed is relevant to your study. If you are not sure if a list item applies to your research, read the appropriate section before selecting a response.

Materials & experimental systems

n/a	Involved in the study
☒	☐ Antibodies
☒	☐ Eukaryotic cell lines
☒	☐ Palaeontology
☐	☒ Animals and other organisms
☒	☐ Human research participants
☒	☐ Clinical data

Methods

n/a	Involved in the study
☒	☐ ChIP-seq
☒	☐ Flow cytometry
☒	☐ MRI-based neuroimaging

Animals and other organisms

Policy information about studies involving animals; ARRIVE guidelines recommended for reporting animal research

Laboratory animals	Experiments were performed on male and female C57BL6N and BALB/c mice, between 8 and 24 weeks of age. All mice were housed in ventilated micro-isolator cages in a temperature-controlled environment (median temperature 23 °C, humidity 60%), under a reversed 11 h dark– 13h light cycle, with ad libitum access to food and water. Mouse cages were changed weekly.
Wild animals	The study did not involve wild animals.
Field-collected samples	The study did not involve field-collected samples.
Ethics oversight	All experimental procedures involving the use of live animals or their tissues were carried out in accordance with the NIH guidelines and approved by the Institutional Animal Care and Use Committee and the Institutional Biosafety Committee at the California Institute of Technology.

Note that full information on the approval of the study protocol must also be provided in the manuscript.